

(NH <sub>4</sub> ) <sub>2</sub> ZnBr <sub>4</sub> Cs <sub>2</sub> MgBr <sub>4</sub>	Rb <sub>2</sub> ZnJ <sub>4</sub> [125,132] Cs <sub>2</sub> CdCl <sub>4</sub> K <sub>2</sub> CoBr <sub>4</sub> [134] Te <sub>2</sub> CoBr <sub>4</sub>	Rb <sub>2</sub> CoJ <sub>4</sub> Tl <sub>2</sub> CoJ <sub>4</sub> [132] K <sub>2</sub> MnJ <sub>4</sub>
	Rb <sub>2</sub> MnJ <sub>4</sub>	
	CS <sub>2</sub> HgJ <sub>4</sub> [133] Tl <sub>2</sub> ZnJ <sub>4</sub>	

Type  $\beta$ -K<sub>2</sub>ZO<sub>4</sub>



#### Chapter 4. Sequence of phase transitions in Rb<sub>2</sub>ZnBr<sub>4</sub> at atmospheric and high hydrostatic pressure.

In this chapter we present the results of studies of phase transitions in Rb<sub>2</sub>ZnBr<sub>4</sub> NQR <sup>79</sup>Br, <sup>81</sup>Br at atmospheric and under high hydrostatic pressure. External exposure is the factor that allows you to get a fundamentally new information about the sequence of phase transitions, in addition to clarify the issues in the form of the NQR lines incommensurate phases.

#### The absorption spectra of NQR <sup>79,81</sup>Br in the incommensurate phase at atmospheric pressure.

When NQR study of compounds with incommensurate phases in which there are significant non-equilibrium processes, it is necessary, in particular, have procedures quantitative measurement of the resonance absorption signal for given values of other parameters (T, t,  $\nu$ , etc.). Such a technique can be designed based on coherent spectrometers. Spectrometer type ISSH the absolute accuracy of the amplitude of the transient resonance signal is small. Therefore, in the research process was used to monitor the intensity of the reference method, which consists in comparing the magnitude of NQR signal recorded at different sample metaequilibrium state, with the value of the equilibrium signal, structural stability of the sample. When working with Rb<sub>2</sub>ZnBr<sub>4</sub> was matched standard, which amounts to less than 10% volume filling of the receiving coil, and the slopes of the temperature and frequency dependences of the pressure of the two NQR lines absorption were sufficient for calibration.

With this methodological technique were significantly clarified the conditions for obtaining reproducible measurements, and also found some side effects. Thus, it was observed that the absolute peak intensity of the NQR signals from the original Br annealed sample  $\text{Rb}_2\text{ZnBr}_4$  increases the amount of accumulation of cooling cycles. However, subsequently, when samples originally uncontrolled contact with moist atmosphere, the intensity of the spectra of incommensurate structure decreases again, and in addition, there is the appearance of three absorption lines, which we have designated  $\nu_H, \nu_C, \nu_B$ . The appearance of these NQR signals, as was explained, due to the excessive influence of atmospheric moisture on the state of the sample. At the same crystal structure of the sample is gradually transformed into another polymorph. Some samples when grown from aqueous solution completely or partially crystallized in this modification, and there is a complete or partial modification of this transition in prolonged contact with moist atmosphere samples.

To elucidate the nature of this phenomenon, measurements were made on the content of crystalline bound water in these compounds, NMR. The results of measurements are structurally bound water (with an accuracy of 2%) was not detected. With the use of X-ray diffraction studies, and considering the NQR signal intensity ratio 1:2:1 (relaxation times are within the time resolution of the spectrometer), it was found that the structural modification ( $\alpha$ ) has the space group symmetry  $P2_1/m$  ( $Z = 2$ ). Upon annealing the samples above 300K structure  $Pnma$  symmetry is restored. Thus  $\beta$ -modification is thermally induced metastable modification of  $\text{Rb}_2\text{ZnBr}_4$ . The frequency dependence of the NQR lines  $\nu_H, \nu_C, \nu_B$  modification  $\alpha$ - $\text{Rb}_2\text{ZnBr}_4$  is presented in Figure 4.1, together with the general progress of other NQR frequency signals from both Br isotopes for  $\beta$ -modification.

In addition to the absorption signals in some cases a special form of the NQR spectrum in the high frequency region of the spectral distribution of the isotope  $^{79}\text{Br}$   $\beta$ -modification ( $\nu \gg 78\text{MGz}$ ) and additional weak lines at the frequencies 79 and 80MHz. These lines, we denote the index of  $\nu_x, \nu_y, \nu_z$  Figure 4.1 and 4.2. As explained, these signals were a homogeneous signals recession free process. Their presence was not related to the existence or absence of the share structure of  $\alpha$ - $\text{Rb}_2\text{ZnBr}_4$  in the samples. Particularly clear signals  $\nu_x, \nu_y$  and  $\nu_z$  manifested after the application to non-hydrostatic deformation patterns. After removal of the load was fixed shape of the spectrum shown in Figure 4.2. As the temperature decreases the frequency of induction of these signals almost coefficients of  $1/\sqrt{T}$ ; 3) the average half-width of the resonance signals latched by spin-echo above  $T_i$  4) The maximum values of the relaxation times  $T_{Q1}$  and  $T_{Q2}$  the position  $\mathbf{I}$   $Pnma$  structure of the compounds studied, where the nucleus of halogens.

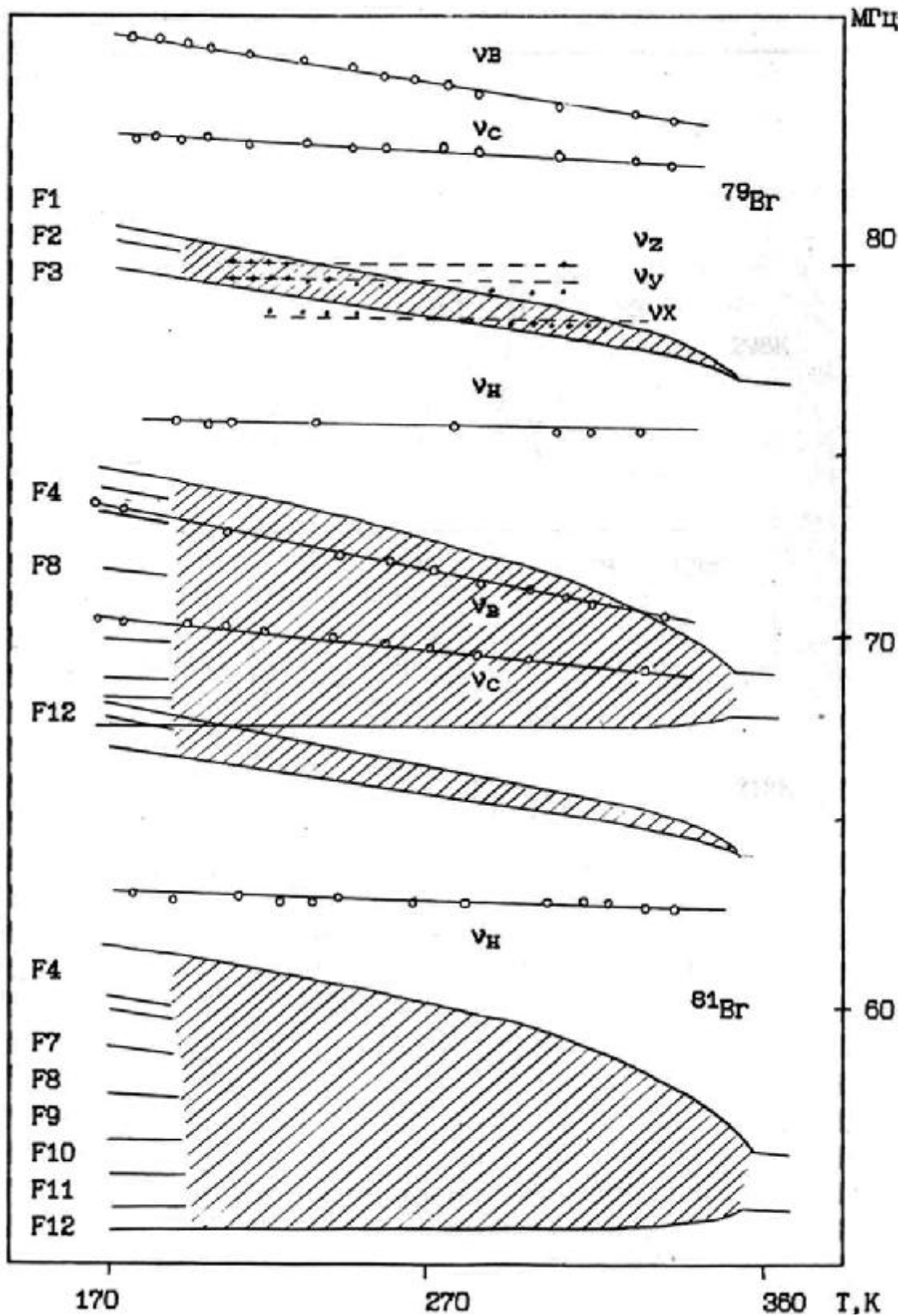


Figure 4.2. View of the  $^{79}\text{Br}$  NQR spectrum from samples of  $\text{Rb}_2\text{ZnBr}_4$  in a stressed state.

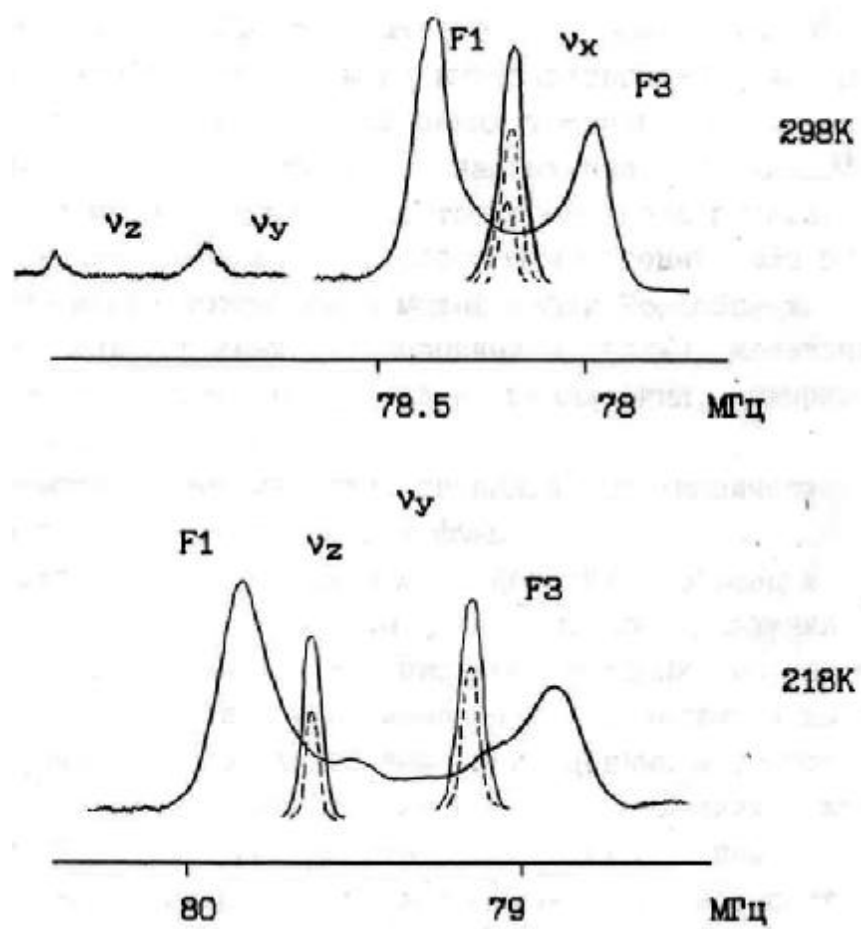
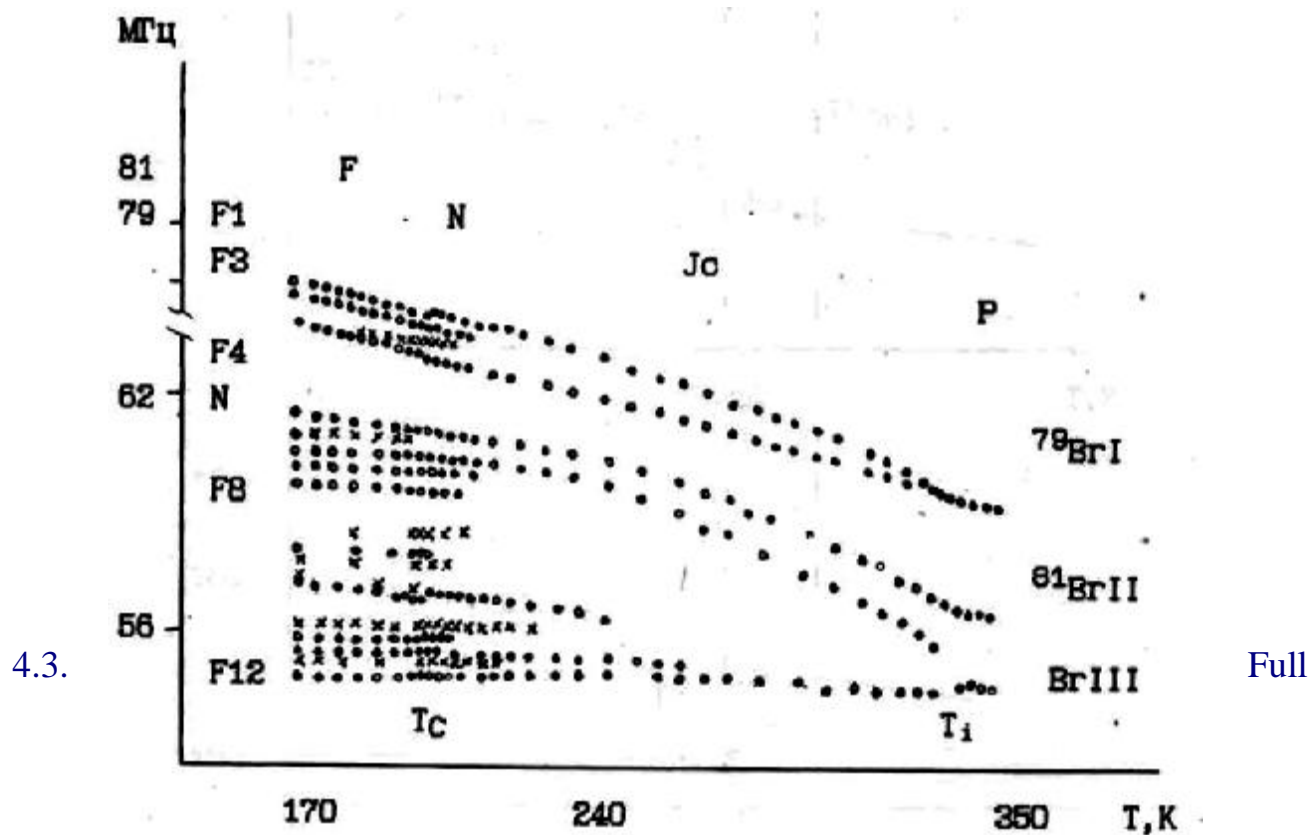


Figure 4.2. View of the  $^{79}\text{Br}$  NQR spectrum from samples of  $\text{Rb}_2\text{ZnBr}_4$  in a stressed state.



temperature dependence of the NQR frequencies Br in  $\text{Rb}_2\text{ZnBr}_4$  at atmospheric pressure.

Explanation of this effect is beyond the scope of this paper. We note only that it can be interpreted as the result of cross-relaxation absorption of certain levels, resulting from nonuniform external voltage with quadrupole levels incommensurate structure tetrabromo zincate rubidium [102].

Thus resulting mining measurements were found:

- 1) Existence of polymorph  $\text{Rb}_2\text{ZnBr}_4\text{-}\alpha$ .
- 2) Impact deformation induced, and also accumulated in the process of crystallization or cooling cycles, the state of voltage samples Jc-phase.
- 3) The dependence of signal intensity on the amount of cooling cycles in the incommensurate phase.

These results were considered in the preparation of samples  $\text{A}_2\text{BX}_4$  to research in atmospheric and high pressure method of optimal matching, to which we shall now describe.

Most of the results of research carried out in the following conditions precluding the manifestation above mentioned effects.

Better signal-noise ratio in terms of liquid-gradient thermal stabilization allowed us to meet precision NQR measurements metastable  $\beta$  modification RZB with an incommensurate phase, to clarify and supplement the results published previously [38]. On Fig.4.3 shows the temperature dependence of the NQR frequencies obtained by the author in the temperature range 390-150K. As can be seen in the high-temperature region near  $T_i$  managed to track more accurately the frequency dependence of the spectral components Br NQR Fig.4.4. Since the frequency of edge peaks of the spectral distribution of the position of the nucleus Br in the Jc- phase lie above the experimental points of the NQR frequency of the nucleus in paraphrase: J<sub>C</sub> phase in the course of the frequency observed in the form of "beak", which is typical for phase transitions with the fluctuation splitting [107]. In the NQR frequencies of nucleus BrI and BrII was monitored more reliable frequency dependence of the splitting. In the region 56MGz below  $T_i$ , we observed a wide frequency distribution, without any trace of the continuum. It was further found that the NQR signals in the paraelectric phase contain both homogeneous and heterogeneous components. In this case the spin-spin relaxation time  $T_{Q2S}$  and  $T_{Q2L}$  of these contributions are at the limit of time resolution of the spectrometer ( $\approx 20\mu\text{s}$ ).

When measuring the width  $T_{Q2}^*$  is most intense line vl, marked difference of its low temperature dependence into a temperature at which the inflection is observed in the frequency dependence of Fig.4.4.

In Jc phase is observed in the behavior of Mild feature spectra, consisting in a slight change in the shape of spectral distributions near 240K. At the same time-frequency spectral shape blurred in 56 MGz (Fig. 3.13) smoothly into a spectral form with three amplitude maximum allowed.

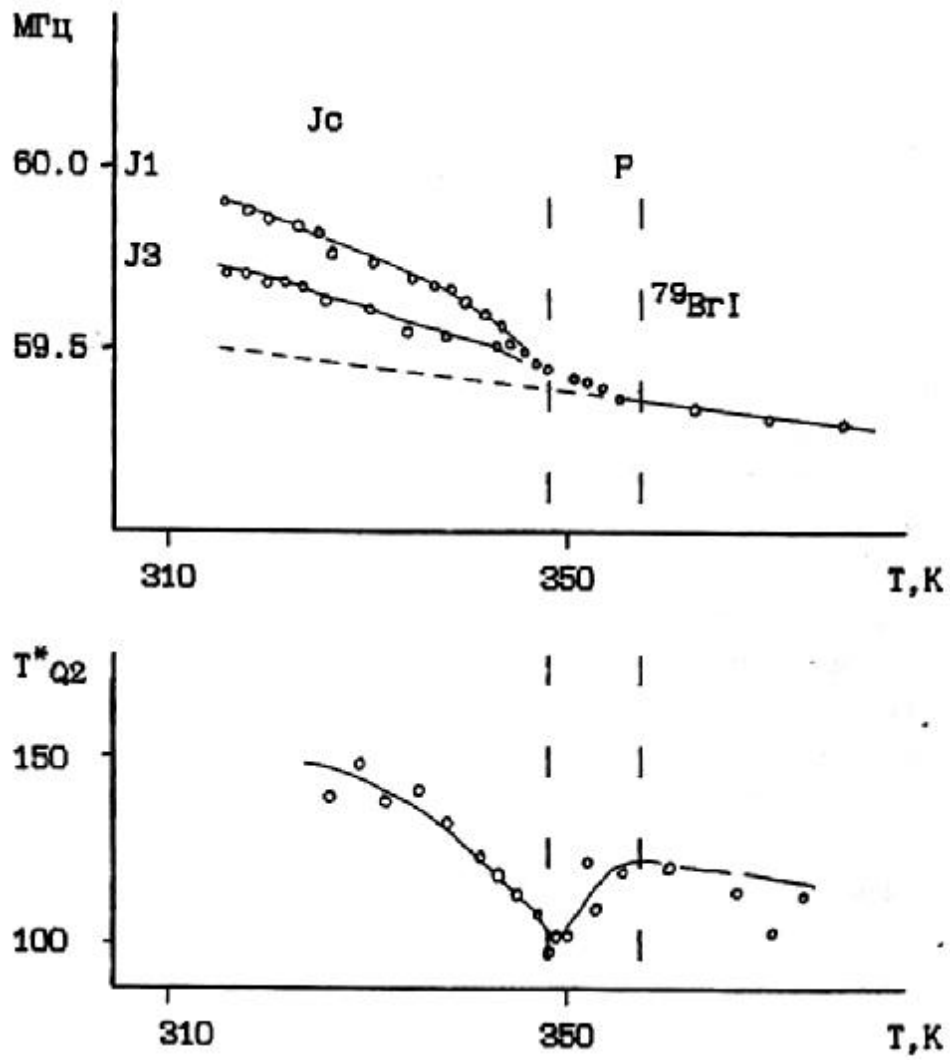


Fig. 4.4. Splitting NQR frequencies the high frequency line and change line width near  $T_i$ .

lg I INT.  
(RLU)

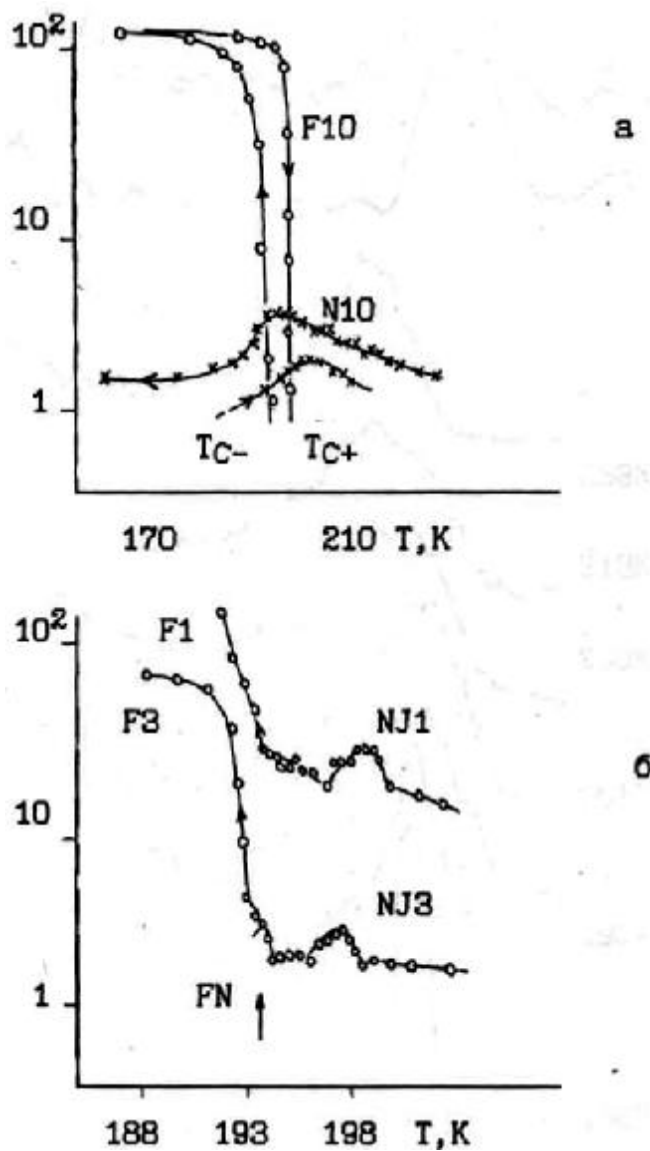


Fig.4.5. Temperature variation of the peak intensities of the lines F, N, and "mixed" type near  $T_c$  in  $\text{Rb}_2\text{ZnBr}_4$ .

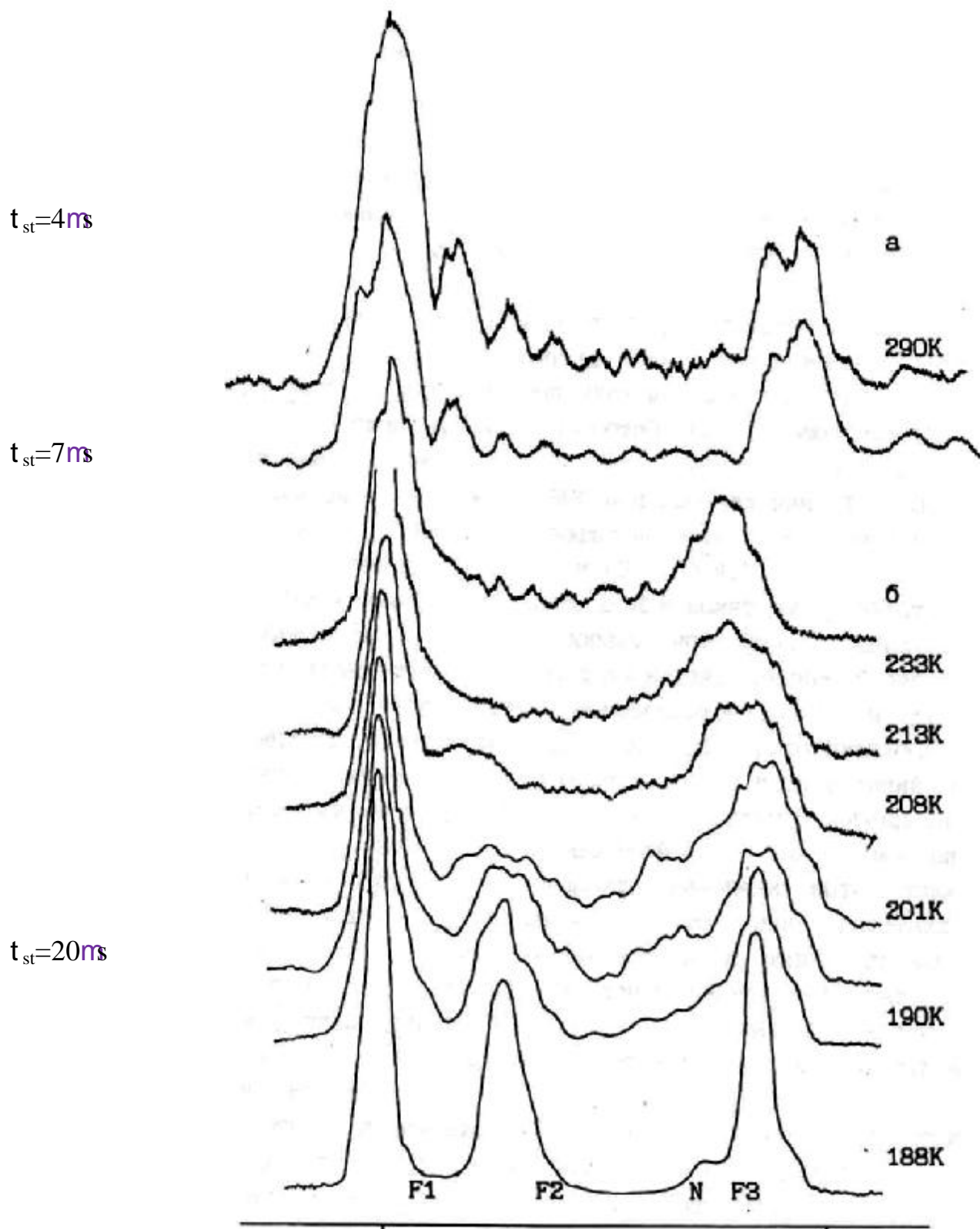


Fig.4.6.  $^{79}\text{Br}$  NQR spectrum of the position BrJ structure with special recording conditions: a) isolation; b) non-isolated gate pulse

Below 220K near  $T_C$  transition in the spectrum detected NQR lines not previously observed. Their frequencies are sufficiently close to the frequencies previously recorded signals. These lines have a smaller intensity and are marked (x) in Fig.4.3 and 4.5a [108,115]. On Fig.4.5 shows the change in the intensity of the line at the frequency  $\nu=56.8\text{MGz}$  (line F10) and lying next to the new line. With decreasing temperature, initially appears and grows in intensity the new component. Its intensity reaches its maximum value to  $T_C$ , stabilized in the 3K and decreases with the passage of  $T_C$ . Appearance and increase in intensity line F10 occurs only near  $T_C$  at  $T \lesssim T_C + 3\text{K}$ . The maximum intensity is achieved below  $T_C - 5\text{K}$  and then remains constant.

Near the high- $T_C$  shape distribution at frequencies 80-78 MHz (Fig.4.6) has at least four components, the central part of the distribution sags to the noise level just above  $T_C$ . The recording of this spectrum (Fig.4.6.) To improve signal performed with great frequency sweep and under  $t_{\text{strobe}} \lesssim T_2^*$  and  $t_2 \gg T_{Q2}$ , so the circuit broad line with a short value  $T_{Q2}$ , oscillations are observed are associated with the apparatus function or gate integrator [126], or with the effects of the polarization of nuclear dynamics [106]. Omitting the finer details of the line profile, we note in this fourth component of the spectral distribution. With precision studies optimal matching method in this mode were obtained accurate temperature frequency dependence of the spectral components of F1-F3 and N NQR spectrum  $^{79}\text{Br}$  Fig.4.7.

Behavior of the intensities of the remaining lines is quite similar to that shown in Fig.4.5, but most of them overlapped with other components of the spectrum, while the temperature-variation of peak intensities of lines located at frequencies overlapping areas, is nonmonotonic Fig.4.56. There is a shift of the NQR frequencies while passing Best  $T_C$  measurement accuracy enabled to detect the temperature hysteresis of frequencies, for example, lines F1 and F3 (Fig.4.7).

This change in NQR spectra can be represented as a transformation of an incommensurate phase lines (lines of type J) through the N-type spectral lines to twelve lines F ferroelectric phase. Lines formed in the immediate vicinity of the ferroelectric phase  $T_C$ , and do not follow continuously through the transition, as it was previously thought [34]. This is most clearly observed in the group of lines F8-F11 and close lying lines N type. In the frequency overlap lines F and N at  $T_C$  recorded small frequency peak races overlap (Fig.4.7). Nonmonotonic behavior of the intensities and frequencies of the lines above  $T_C$  indicates that they are unresolved frequency overlap lines F and N-type (spectral lines overlapped FN type), and at higher temperatures are covered by other types of lines N and J (NJ line type). Last gradually converted to the spectrum of the middle region of the incommensurate phase (Fig.4.8).

These experimental data and data on the measurement time  $T_{Q1}$  quadrupole spin relaxation of Br [103, 109] indicate the need to revise the model proposed in [34] to describe the shape of the nuclear resonance line in incommensurate phases. Fixed structure of the spectrum allows for the interpretation of the line shape in the framework of the existence of long-period structures. In this case, using the expansion of the atomic displacements on the eigenvectors of the soft mode (1.1) we have:

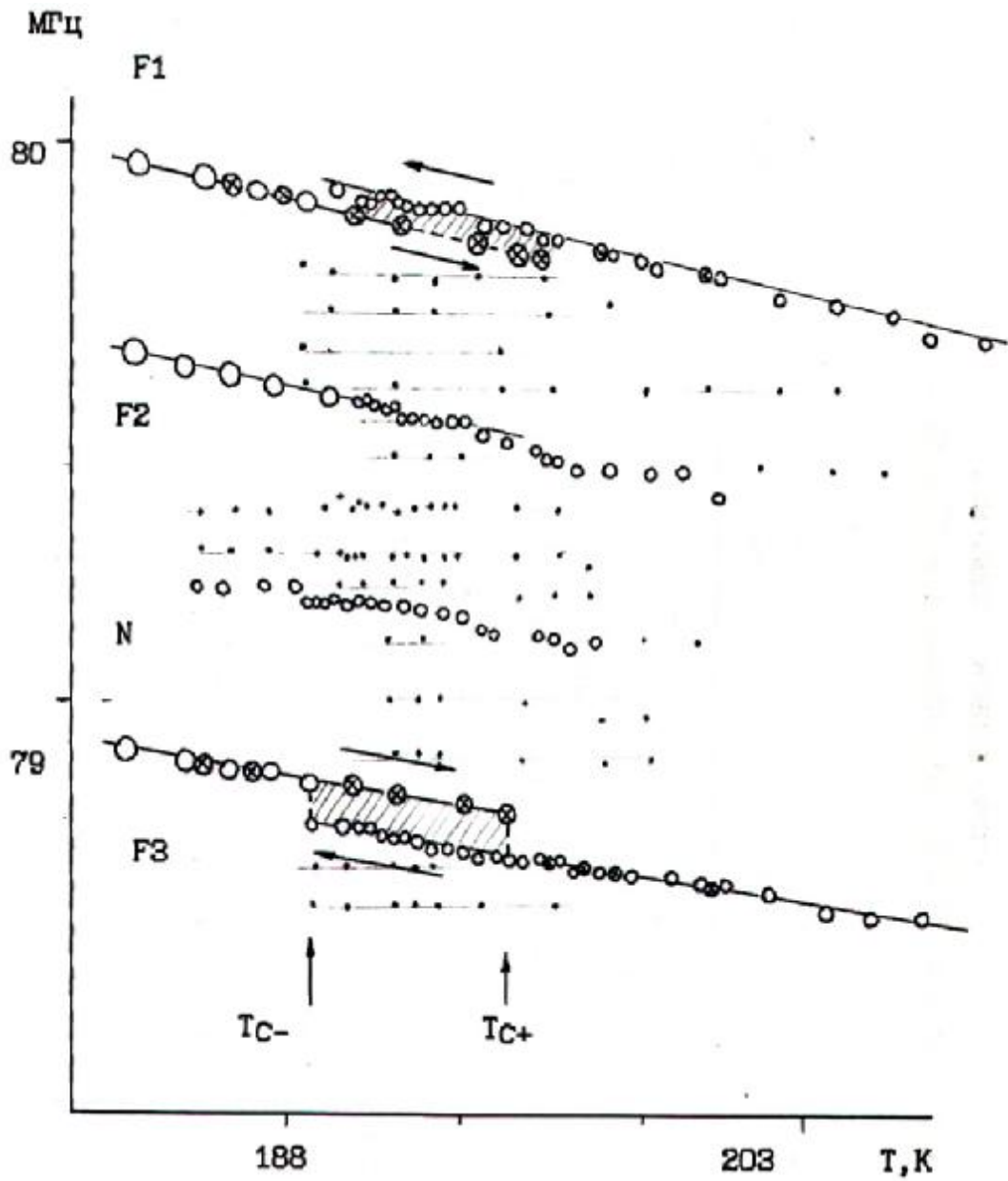


Fig.4.7.

and the

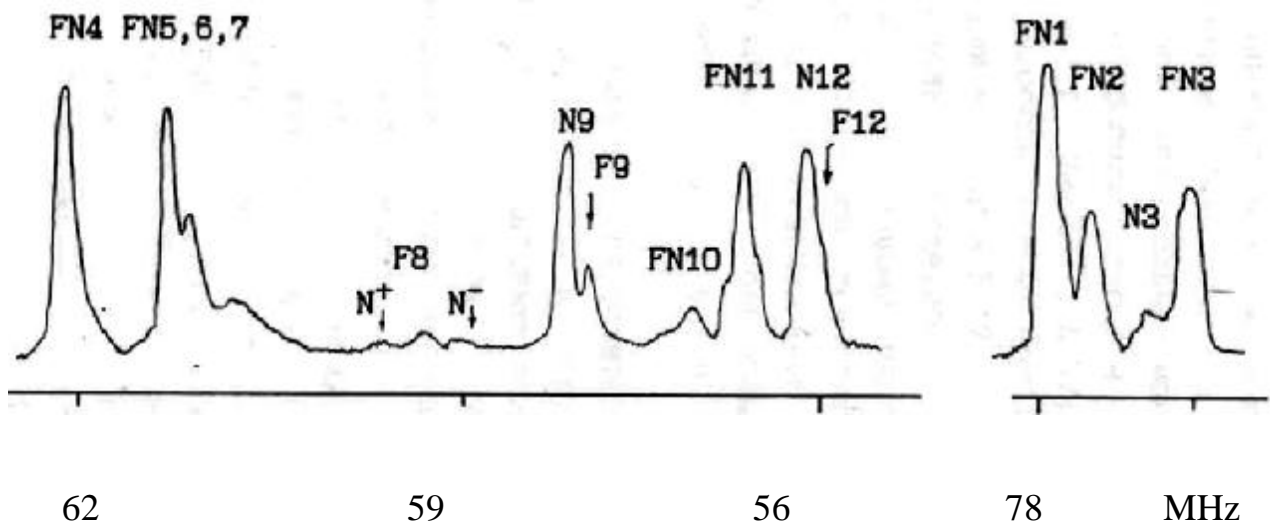


Fig.4.8. View NQR spectrum near  $T \gg T_C + 2K$  at atmospheric pressure.

$$u(\mathbf{k}p) = \prod_{\lambda=1}^L A_{\lambda} \exp\{-2\pi i(\frac{N}{M} \mathbf{q}_S \cdot \mathbf{x}_{\mathbf{k}} - \varphi_1)\} \dots \quad (4.1.)$$

Spectral density function (1.33) is discrete, and the shape of the line will be the sum of the spectral components of the form  $g(\mathbf{v})$ . Taking the calculation of expression (4.1) and in the simplest case, we only consider one rotational mode  $S_{10}$  ( $A_1^1$  local approximation,  $L = 1$ ), we calculated the shape of the lines of the long-period structures such as 3/11; 5/17; 9/29; 11/35, with varying angle  $\varphi_0$  in shirokovolnovom approximation. In Figure 4.9 shows an example calculation for modulating 5/17 with different values of  $\varphi_0$ . Increasing the width of the original singlet component  $g(\mathbf{v})$  line shape is close to the continuous frequency distribution (dashed line). At room temperature, the estimated line may be adjusted by experimental verification of the continuum on the assumption that modulation of the 5/17 simultaneously coexists with different values of the phase angle  $\varphi$  and introducing corrections relaxation contour line.

In the low temperature region, where the soliton tapered wall and the main structure similar to the crystal structure of the ferroelectric phase to the value of  $q_d = 1/3$ , we shall use the expression for the non-linear phase angle  $\varphi$ . The calculations in this case showed that a satisfactory agreement with the experimental line shape can obtain if modulations along with close to 1/3 (5/17, 3/10) briefly introduce a periodic modulation of 1/4, which is indispensable in the local approximation to describe the fourth component spectrum. This assumption means that an increase in the contribution from other modes of symmetry, such as  $S_3$ , or from a different view, for example,  $A_q$  [93],  $S_2$  fashion, formally analogous to the introduction of non-local description. On Fig.4.10 shows the calculated line shape is obtained by assuming the coexistence of the modulations with wave vectors 3/10 and 1/4, respectively, taken with weights 4:1:1:2. The coincidence of the calculated and experimental forms, as can be seen from the figure, is quite satisfactory.

Thus NQR data at atmospheric pressure indicate that near  $T_C$  structure of the incommensurate phase of  $\text{Rb}_2\text{ZnBr}_4$  can be represented by the coexistence of multiple modulation sequence "satanic stairs. This is not inconsistent (X-ray diffraction data. [110] However NQR data indicate that besides the modulation of 1/3 must be present for at least another one even short-modulation.

For the experimental confirmation of the existence of such a structure, it was decided to expand the area of research through additional parameter - the external hydrostatic pressure. When this was to be expected that in the "devil's staircase" this will change the proportion of one phase at the expense of others, and to facilitate their supervision.

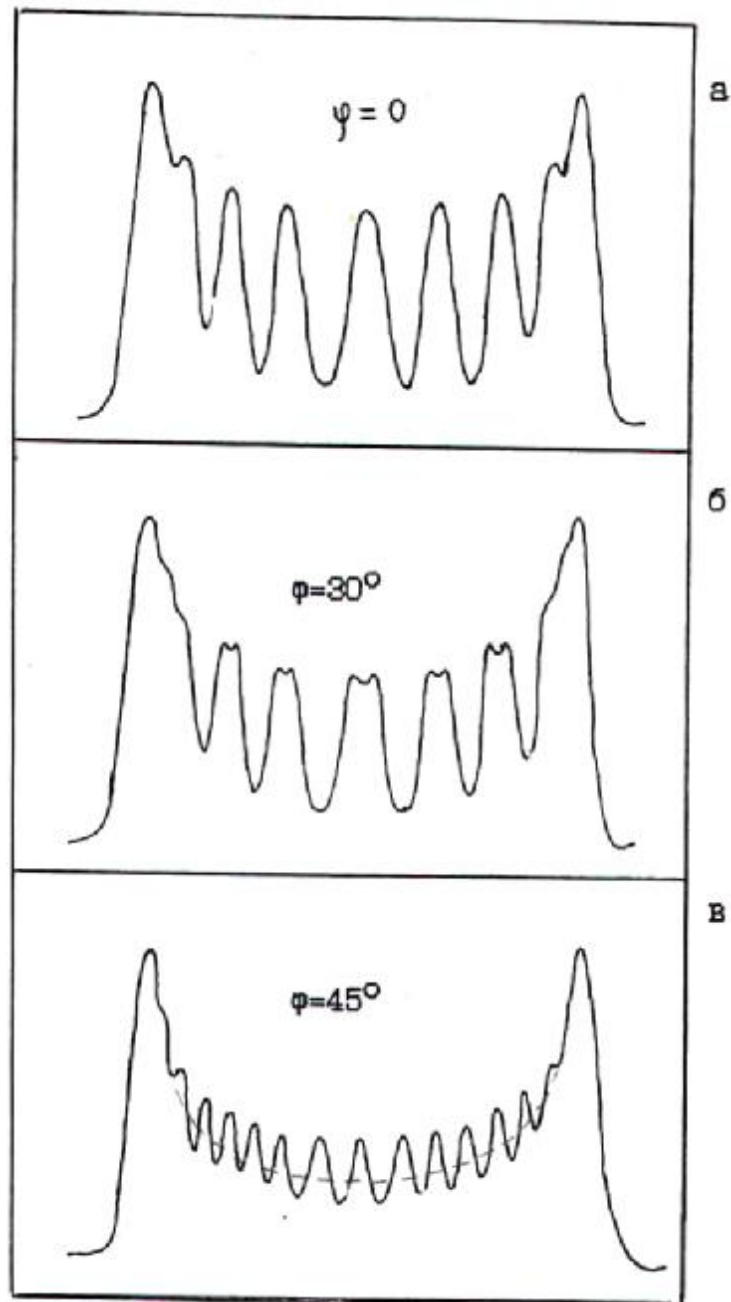


Figure 4.9. Calculated line shape in the long-periodic approximation  $M/N = 5/17$ ;  $A_q = 0$ .



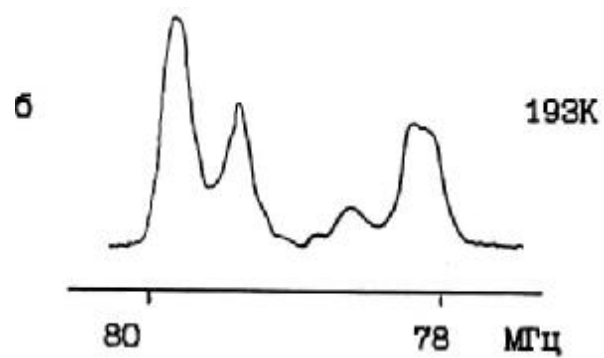


Fig.4.10 a) Calculated line shape in the long-period approximation Coexistence modulations third;  $3/10$ ,  $1/4$ ;  $5/17$ ; respectively, with weights of 4:2:1:1 ( $A_q = 0$ );  
b) Experimental

### P-T phase diagram of $\text{Rb}_2\text{ZnBr}_4$ .

In the beginning of this section briefly touch on issues of experimental measurements techniques not mentioned in Sec. 2. During the first stage, which was carried out in 1986-87, decided camping methodical task is to determine the possibility of equipment to record the "disproportionate" spectra at high pressures and determine increases or decreases the temperature range of the existence of  $J_c$  structure to such impacts [136,137]. This problem was originally solved by a high-temperature phase transition area using a titanium chamber NQR method and differential thermal analysis (DTA construct a cell for measurement is described in [74]). At temperatures below room used low-temperature cell HPC1. And only later, after the production of the second stage HPC2 managed to meet the challenge of a detailed study of structural changes in the  $J_c$  phase. In the study technique was used isobaric and isothermal changes of P-T parameters. The spectra were recorded with a temperature step of 5-10K and step pressure of 0.1-0.5 MPa. Frequency scanning range was from 55 to 78MGz. To control the sensitivity of the receiving path and to assess the impact of non-equilibrium processes in crystalline amplitude spectrum used NQR "frame". P-T field of study in HPC2 was 170-290K at pressures up to 0.4 GPa. Above these pressures and temperatures data obtained HPC1. Total about 20 iso-sections. tracked, recorded more than 300 spectra. The samples of high quality obtained with the growth of single crystals for NMR experiments. Due to the fact that data obtained in HPC2 far been published only in a succinct form, we elaborate on their description in this paper.

On Fig.4.11 open circles marks the position of the differential thermal break in the temperature curve passing P- $J_c$  transition at different pressures. For comparison, in this figure, dotted line plotted P- $J_c$  transition obtained later by Japanese researchers according dielectric measurements [59]. Note that the phase transition temperature  $T_i$  and DTA recorded at atmospheric pressure differ by more than 5K.

NQR measurements in the area of  $T_i$  conducted on high-line absorption signal from nucleus BrI.

(Presented below is a purely technical information intended for trainees and specialists experimenters. Panoramic reader can omit these routine details and go to end of this section.)

When isobaric changes in the phase transition observed "failure" in the intensity of this line, and at higher pressures, the line was not observable in a greater range of temperatures. These intentions have shown little promise HPC1 use design with a small diameter of the working channel for research NQR spectra near  $T_i$ . However, it was found that the temperature  $T_i$  with increasing pressure shifts to the high temperature region and the phase transition is smeared P-I (Fig.4.11).

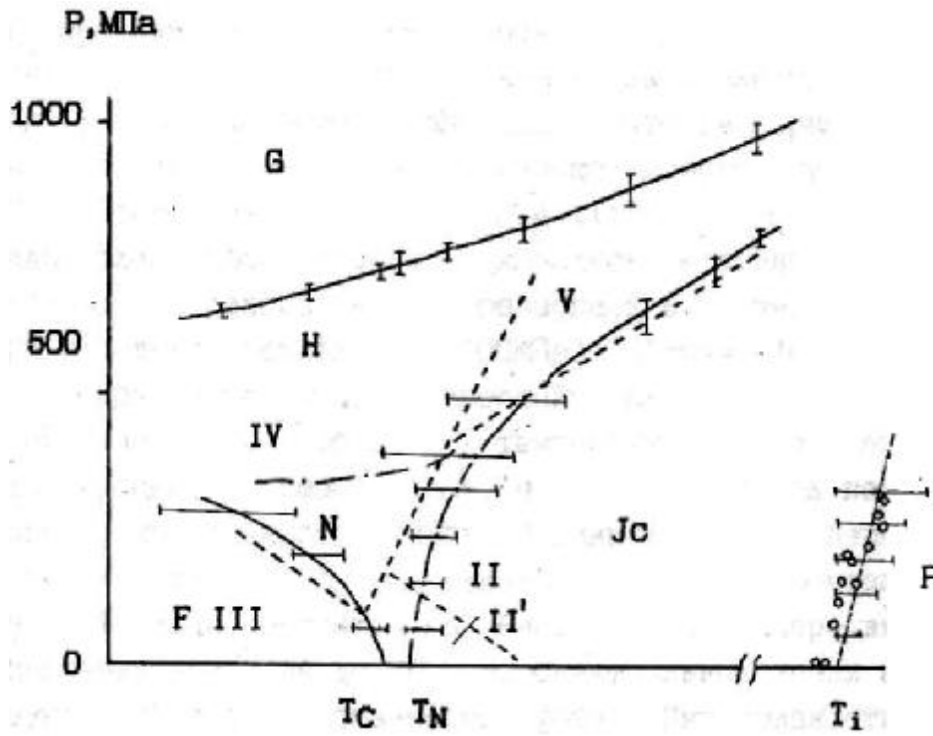


Figure 4.11. DTA data (open circles) near  $T_i$ , dielectric [59] (dotted lines, Roman notation) and NQR (continuous lines) measurements in the  $P$ - $T$  region of the incommensurate phase of  $\text{Rb}_2\text{ZnBr}_4$

lg I (RLU)

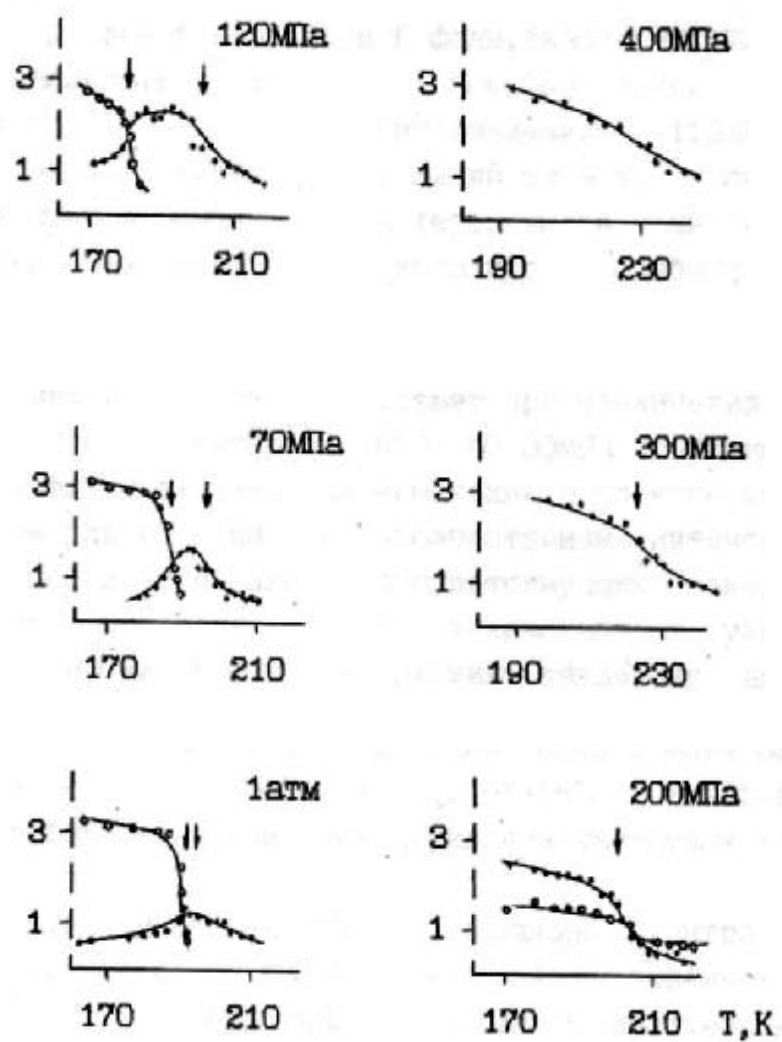


Fig.4.12 The relative intensity of the spectral lines NQR F10 and N10 at different pressures.

Much more informative studies were NQR in the transition from the incommensurate to the ferroelectric phase. At low pressures 100MPa near  $J_c$ , there was a marked increase in the intensities of the NQR lines of type N. With increasing pressure, the temperature region where these lines appear in the spectrum, expanding that recorded by changes in relative intensities of the "clean" lines of type N, NJ overlapped and FN and F types of spectral lines. The relative intensities of the course is illustrated by the example of Fig.4.12 lines F10 and N10. In the pressure range up to 250MPa. The spectral lines of these types coexist in the incommensurate phase. Intensities of the lines of type N increases gradually and at pressures higher than 250MPa spectrum consists of 14 discrete lines, which were correlated with the existence in this pressure commensurate phase N.

In isobaric measurements at 200MPa with decreasing temperature, a phase transition to the ferroelectric structure, which is characterized by intense 12 discrete absorption NQR (line F1 - F12). With increasing temperature above 210K spectra intensity gradually decreases. Area of P-T parameters (where the overall intensity of the spectra decreases) designated by us  $J_c$  symbol on Fig.4.11 can be roughly separated from the rest of the low-temperature region of the incommensurate phase.

During the measurements, it was also found that the isobaric passages corresponding to high pressures from the incommensurate phase transitions ( $J_c$ ) in the N phase and ferroelectric phase strongly blurred. Changes in the intensities F, N and overlain groups of lines are so gentle that above 150MPa definition phase transitions becomes difficult. Fig.4.11 on the phase diagram based on the results of isobaric studies [116,118,136,137]. Experimental data suggest the possibility of a more complex structural changes in the N phase. These assumptions were confirmed by us in isothermal studies CPH2 [111,112,116], for a detailed exposition of which we proceed.

Increased pressure in the F phase (isotherm 173, 183 and 188K) possible to observe the following transformations NQR spectra: Fig.4.13, 4.14 and 4.16. Pressures up to 90-110MPa observed only 12 lines of F type. Traces type lines N, due to the lower sensitivity in a bomb than a heat chamber, is not recorded. The above values range complemented weak spectral lines of type N (shaded areas on the spectrum Fig.4.13 and 4.14). Their intensity increases with increasing pressure to ~ 150MPa, and further in the range of DP ~ 60, 30MPa stabilized. With further increase of pressure changes in the spectrum are characterized by the disappearance of the lines of type F, increase the intensity of the N lines and the appearance of lines corresponding phase H: H-lines. Intensity increases dramatically past a narrow range of pressures above 250, 280MPa and at higher pressures there is powerful resonance lines 14, two of which, at frequencies 65.8 MHz and 66.7 have twice the strength.

On Fig.4.15 presented as an illustration of the baric stroke frequency of the NQR spectrum of  $Rb_2ZnBr_4$  at  $T = 183K$ . In the phase transition region the slope of the frequency of moves and jumps NQR frequencies.

Features isothermal evolution of the spectrum in the P-T field is an extension of P-interval overlap (coexistence) lines of type F and N with increasing temperature isotherm. So at 189K coexistence region F and N spectral lines is about 30MPa at 188K 40MPa and at 173K - £10MPa. However, the transition to the isobaric change in temperature in the range 160-200MPa, the coexistence lines of type F, N and H extends over a wide temperature range over 40K and 200MPa isobar on phase transitions in H or F phase was not observed up to 150K. These data indicate that the region of coexistence the phases

183K

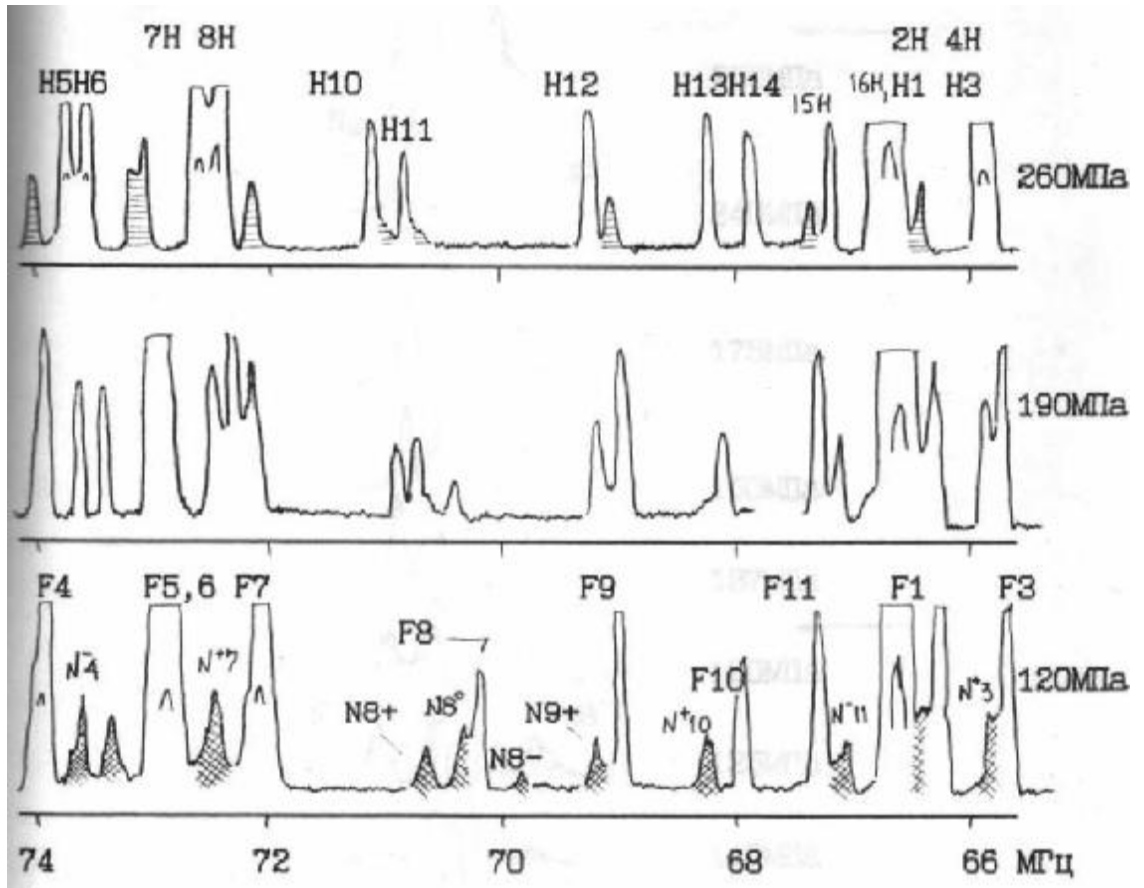


Fig. Full Br NQR spectrum in RZB at T = 183K and different pressures.

Rb<sub>2</sub>ZnBr<sub>4</sub>  
183K

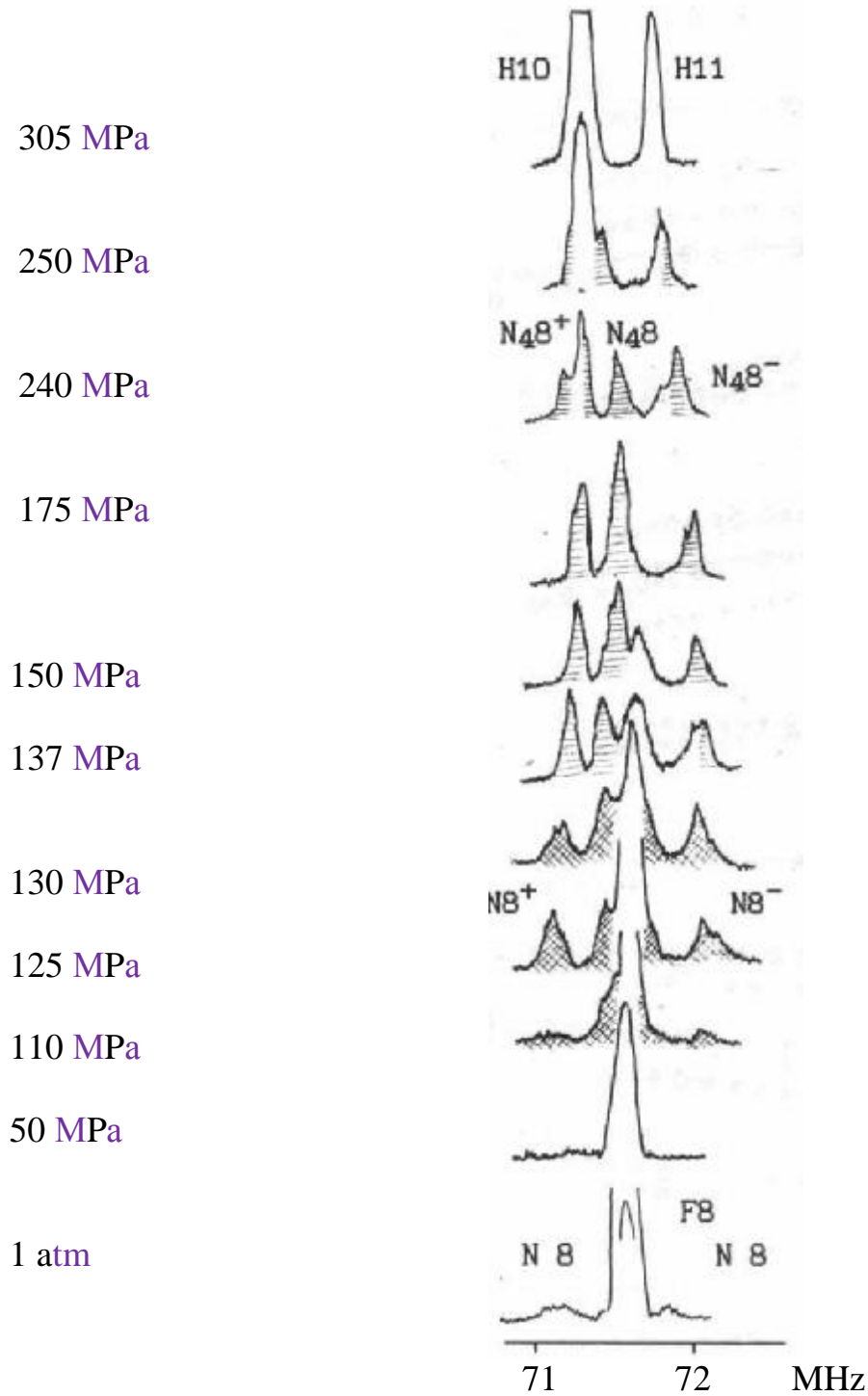


Fig.4.14. Changing of the NQR spectrum with increasing pressure at T = 183K.

4  
MHz

74

71

68

66

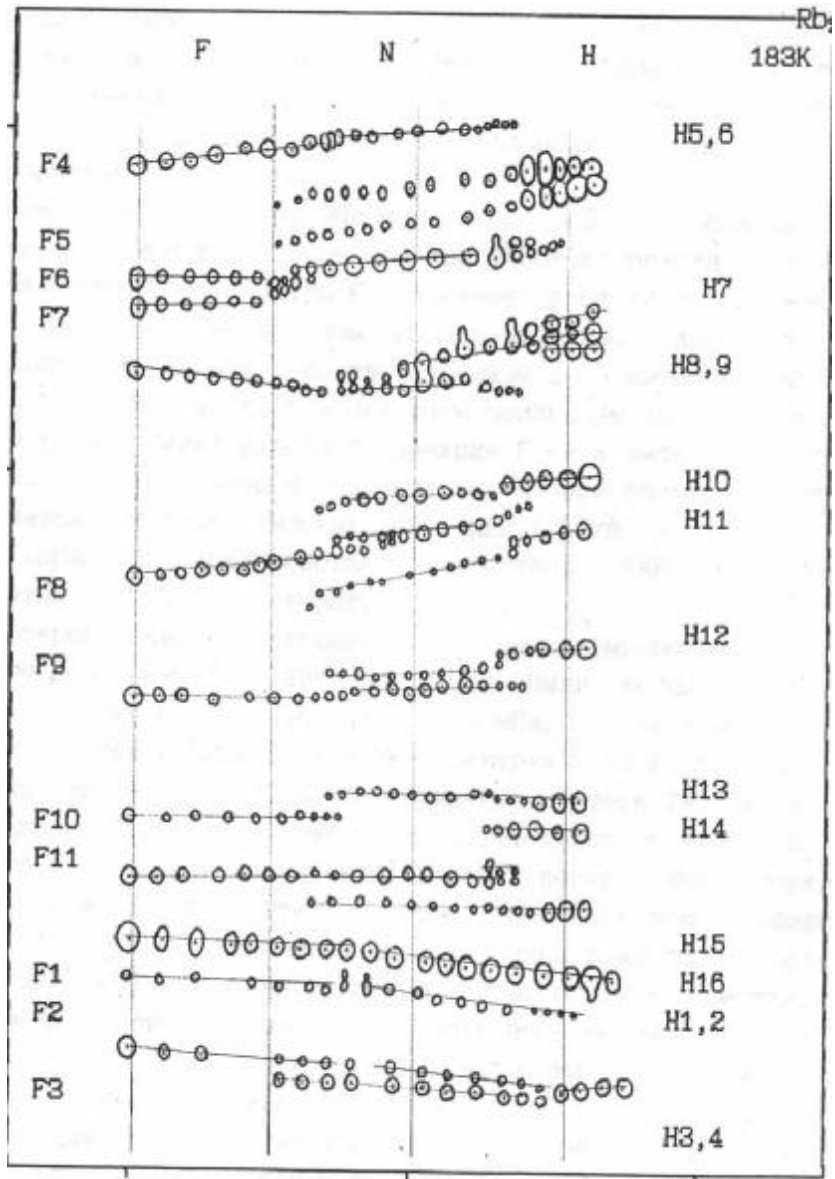


Fig. 4.15. Baric stroke line frequencies of the NQR spectrum at T = 183K.

dependent on the direction of change of the parameters P- T in relation to the P-T-phase lines.

As the pressure decreases from phase H hysteresis of phase transitions. To move H  $\leftarrow$  N DP 20 , 40MPa, the transition F  $\leftarrow$  N DP from 30 to 60MPa where value increases with increasing temperature.

Thus isothermal method at low temperatures clearly recorded two phase transitions F $\leftarrow$ N and N $\leftarrow$ N. Multiplicity NQR spectrum varies from 12 lines of singlet type F, through no less than 20 spectral lines of N type to sixteen NQR lines, corresponding to the high pressure phase N. Both phase transitions in classical featured are first-order transitions. Phase transition line F $\leftarrow$  N is negative  $\frac{dP}{dT}$  Phase transition H $\leftarrow$  N at high temperatures observed at higher pressures ( $\frac{dP}{dT} = 2,86$  MPa/K) with a character transformation spectra NQR does not change significantly at temperatures up to 210K.

Isothermal studies in the field of low-temperature incommensurate phase (from 189K to 200K) were performed in detail with step 10 , pressure 50MPa. Let us consider the general patterns observed in the NQR spectra in this area.

On Fig.4.16 and 4.17 for example isotherms T = 198K and T = 190K presented baric Frequency spectrum lines. Due to the fact that in this area of P-T observed spectral distribution with a complex change in intensity on the pressure dependence (Fig.4.17), except for specifying the frequency of the peak of each distribution, a closed oval contour scheduled spectral distributions that reflect their intensity and area of overlap. On Fig.4.26 and 4.27 are graphs of peak intensities. With increasing pressure, the overall intensity of the spectra increases and decreases the half-width frequency distributions. At a certain pressure, in the absence of frequency overlap, have seen the emergence of new lines (for example N8<sup>+</sup>, N8<sup>-</sup>, N11<sup>+</sup>) Fig.4.17. P-T boundary area of occurrence of these lines at high temperatures is shifted to higher pressures and the phase diagram it is possible to compare a certain P-T line at = 150MPa and 200K (Fig.4.24). When crossing this line is also measured the change in peak intensities most NQR signals. With decreasing, the pressure indicated hysteresis in the position marked abnormalities DP 40MPa.

Thus, all indications in phase N, a phase transition from a phase existing near atmospheric pressure to a phase N4, the previous high-symmetry phase N. A detailed analysis of the spectral data (see § 4.3) shows that the evolution of the NQR spectrum in the P-T region is represented by a more complex way than the coexistence of spectral lines F, N or HN type. At pressures of ~260MPa, clearly observed phase N $\leftarrow$  H transition.

We now describe the data in isothermal studies CHP2 in the middle region of the incommensurate phase (above 200K). The characteristic form of NQR spectra in this area is presented in Fig.4.18. Fig.4.19 on the example shows a typical isotherm 219K baric frequency dependence of NQR lines, and change Fig.4.20 peak intensity spectral component at the frequency J14 - 67.3 MHz, which is characteristic for the other lines of the spectrum.

At atmospheric pressure, the shape of the spectrum is represented by a small number of resolved components (Fig.4.18a). This form is maintained until the pressure 200MPa, where there is the first anomaly. So blurred spectral distribution at frequencies 69, 66,5 MHz (line group conventionally designated J13-J16) above 200MPa varies considerably (Fig.4.18b). Shape of the spectral distribution J5-J6 and J7-J8 also converted by increasing the circuit under their new spectral components. Group lines J1-J4, at atmospheric pressure characterized by a continual distribution between edge peaks above 200MPa

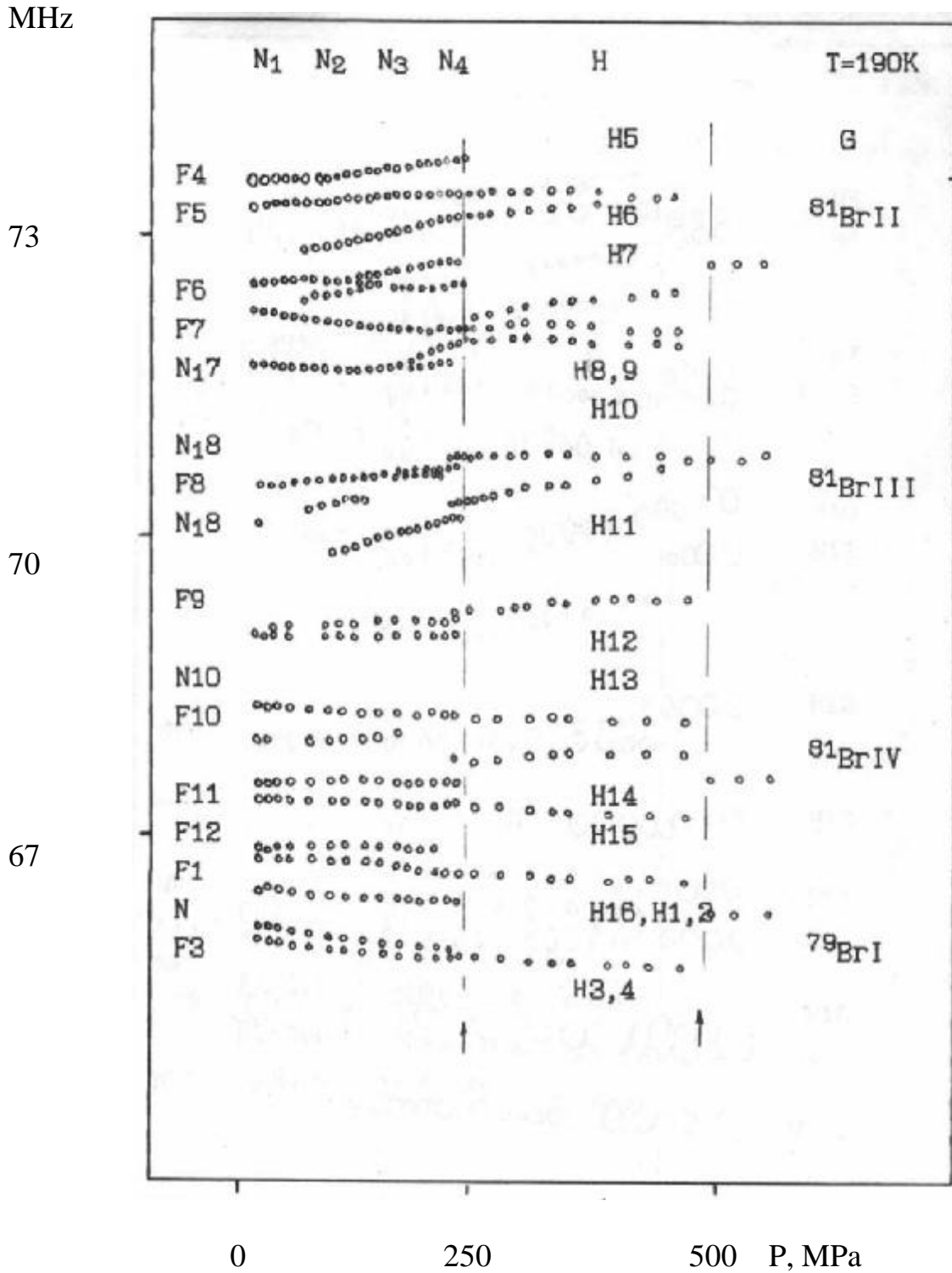


Fig. 4.16. Baric move NQR frequencies at T = 190K.

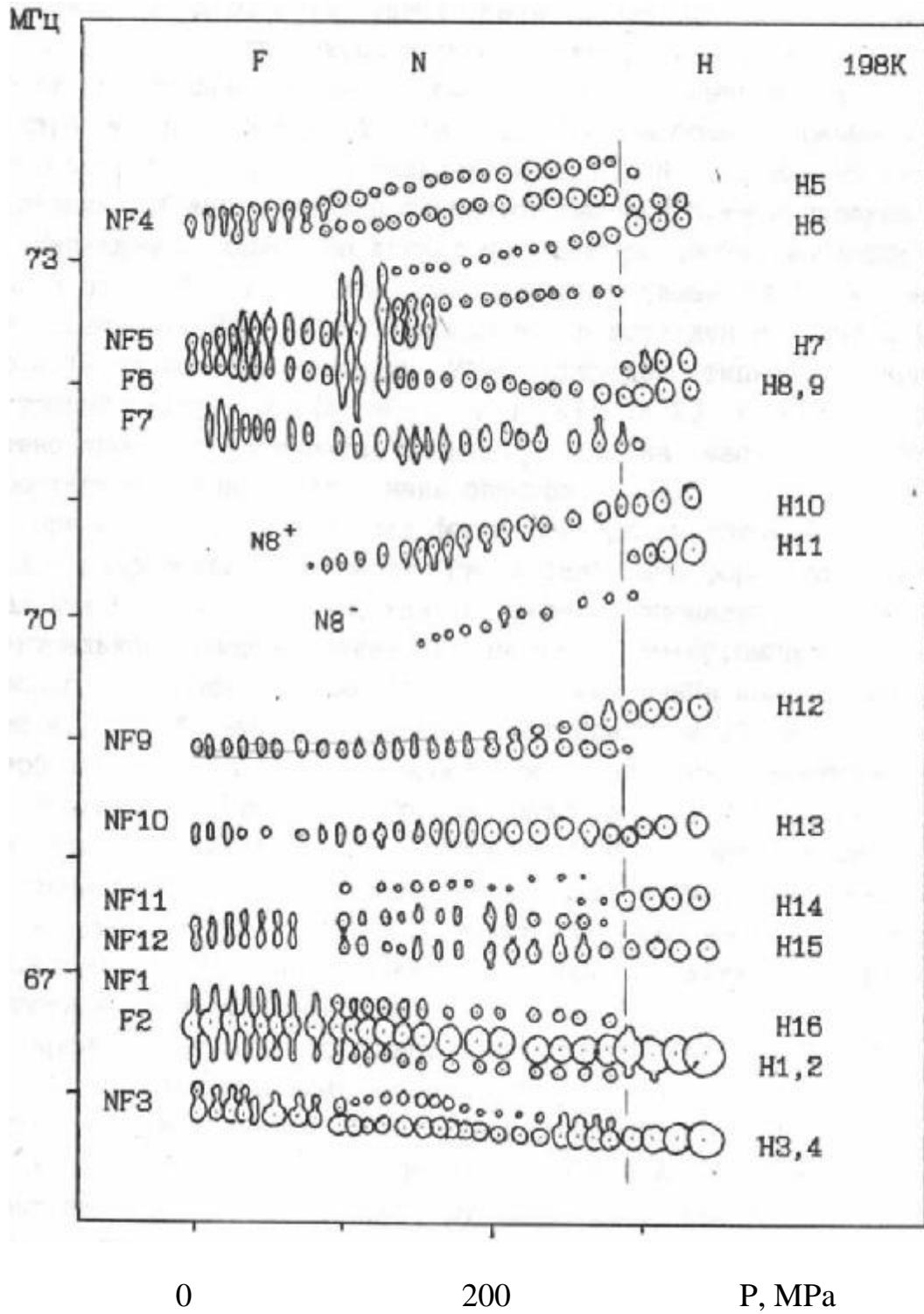


Fig. 4.17. Baric move NQR frequencies at  $T = 198\text{K}$ .



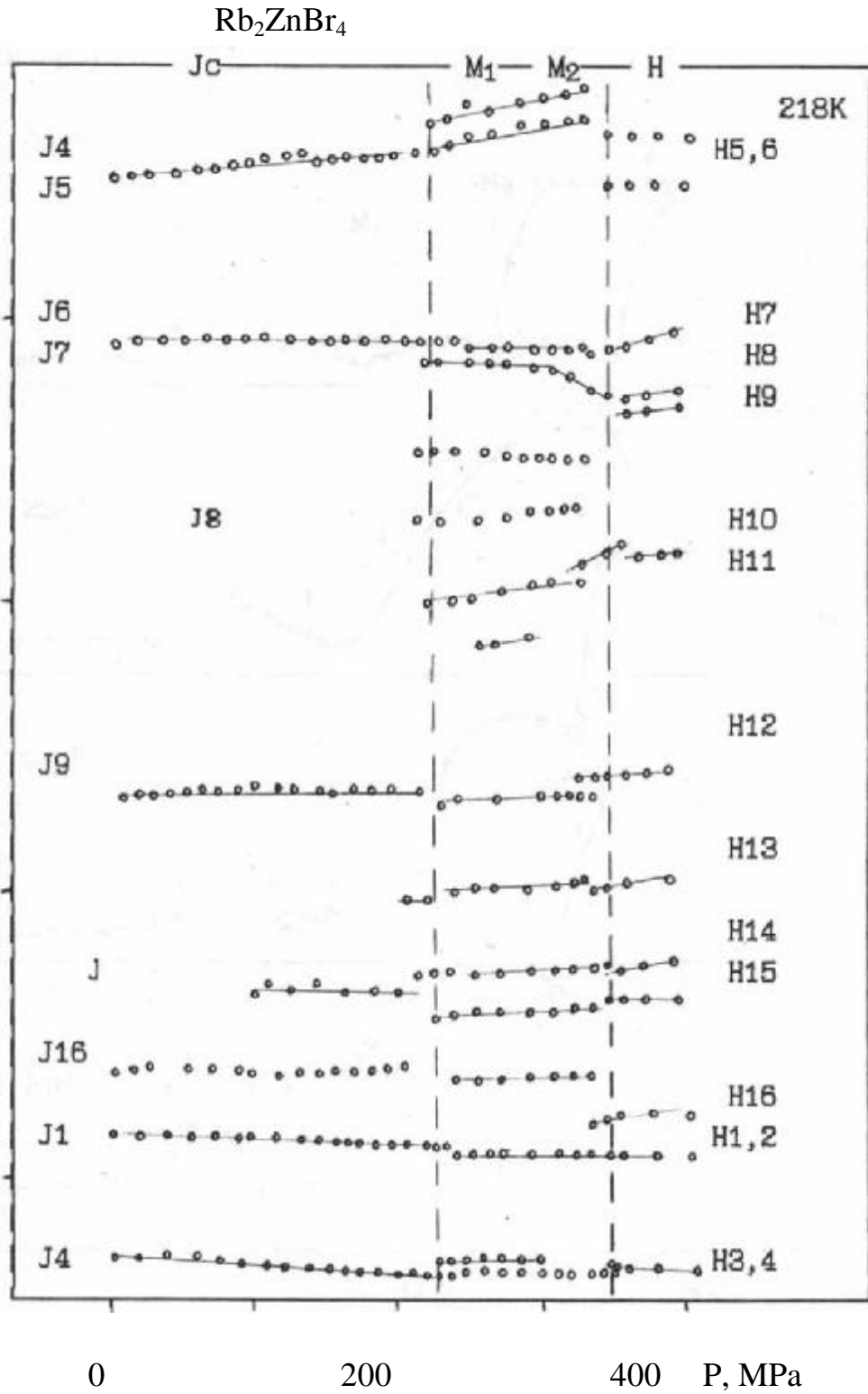


Fig.4.19. Baric move NQR frequencies at  $T = 218\text{K}$ .

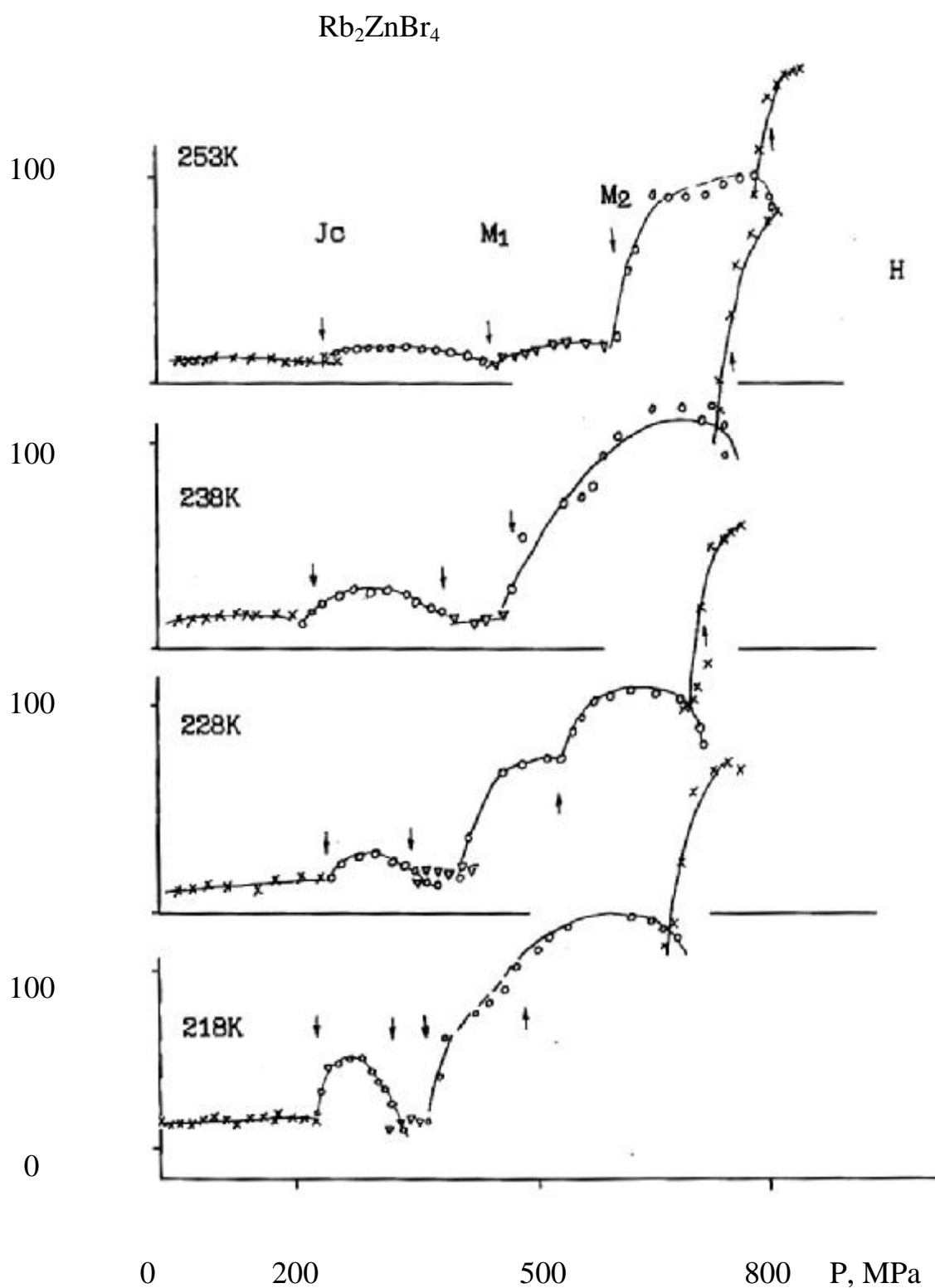


Fig.4.20a-g. Baric change in the intensity of the spectral lines NQR type J4-M14 at different temperatures.

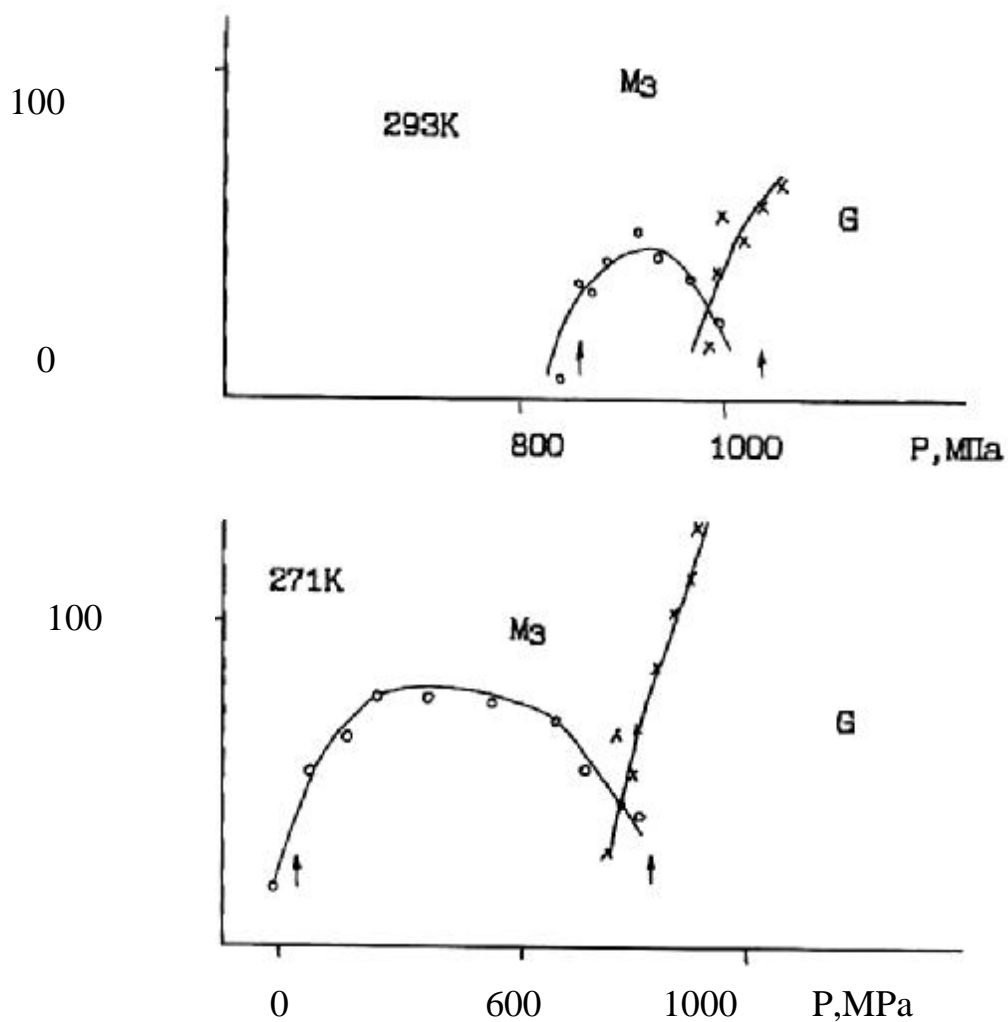


Fig.4.20d th. Baric change in the intensity of the spectral lines NQR type J14-M14 at different temperatures

proceeds to the frequency resolution of the form M1 - M4. Absorption signals at frequencies 70-70,5 MHz observed only above 200MPa, and at high temperatures in all of high pressures.

Also noticeable transformation of the spectrum shape (Fig.4.18a and 4.18b) measured the change in the half-width distributions and their peak intensities (Fig.4.20). Thus, a phase transition from a phase of Jc to a new phase marked by us symbol M1. With increasing temperature recorded overall reduction ratio S/N Features characterizing the anomaly Jc« M1 becoming less distinct and isotherm 250K completely blurred. When the pressure is reduced there is a significant hysteresis of the phase transition Jc« M1 about DP 160MPa. Fig.4.24. Marked change in the slope of the phase transition to negative  $\frac{dP}{dT} = -75\text{Pa/K}$ .

As the pressure increases in this temperature range by a second anomaly. It is characterized by changes in the forms of spectral distributions (Fig.4.18g and 4.18v), especially during the peak intensities of all lines (Fig.4.20), as well as a notable change in the frequencies of spectral peaks and slopes of the frequency dependencies (Fig.4.19).

Transition into a new phase, which we denote by M<sub>2</sub>, with increasing temperature isotherm is shifted to higher pressures with a positive slope with respect to the temperature axis  $\frac{dP}{dT} \gg 110\text{Pa/K}$ . At temperatures above 260K transition line M<sub>1</sub>« M<sub>2</sub> is not tracked due to the excess of its intended position limit values HPC2 pressure, and in the case HPC1 not sufficient sensitivity of the apparatus. Hysteresis transition M<sub>2</sub>« measured isotherm 211K is about 50MPa.

When pressure rises above 400MPa width of the spectral distributions decrease at a certain pressure and intensity of the NQR lines increases sharply, then stabilized again (Fig.4.21 and 4.22). There is a new spectral line frequency offset with respect to the spectral lines of phase M<sub>2</sub>. This spectral anomaly, we compared with the phase transition into the next phase of high pressure M<sub>3</sub>. Position of the transition points determined from the inflection in the course of baric intensities of the NQR lines M12-M16 (Fig.4.22). At high temperatures, the anomaly in the transition M<sub>2</sub>« M<sub>3</sub> is fixed much clearer. The slope of the transition line between phases M<sub>2</sub> and M<sub>3</sub> is  $\frac{dP}{dT} = 8\text{MPa/K}$ . Hysteresis transition DP  $\gg 40\text{MPa}$ .

Thus, when the pressure in the middle of the incommensurate phase observed sequence of phase transitions J« M<sub>1</sub> « M<sub>2</sub> M<sub>2</sub>« M<sub>3</sub> The decrease in the width of the spectral lines indicates the ordering of the incommensurate structure with increasing pressure.

With increasing pressure above 500MPa, or with decreasing temperature below 250K in this P region, the shape of the NQR spectrum continues to change (Fig.4.23) and transformed to characteristic of phase N. Due to the large step measurements (5-10K, 50MPa) in the P-T range, and the vagueness of the anomaly, the proposed line separating phase M<sub>3</sub> and H is fixed with a large error.



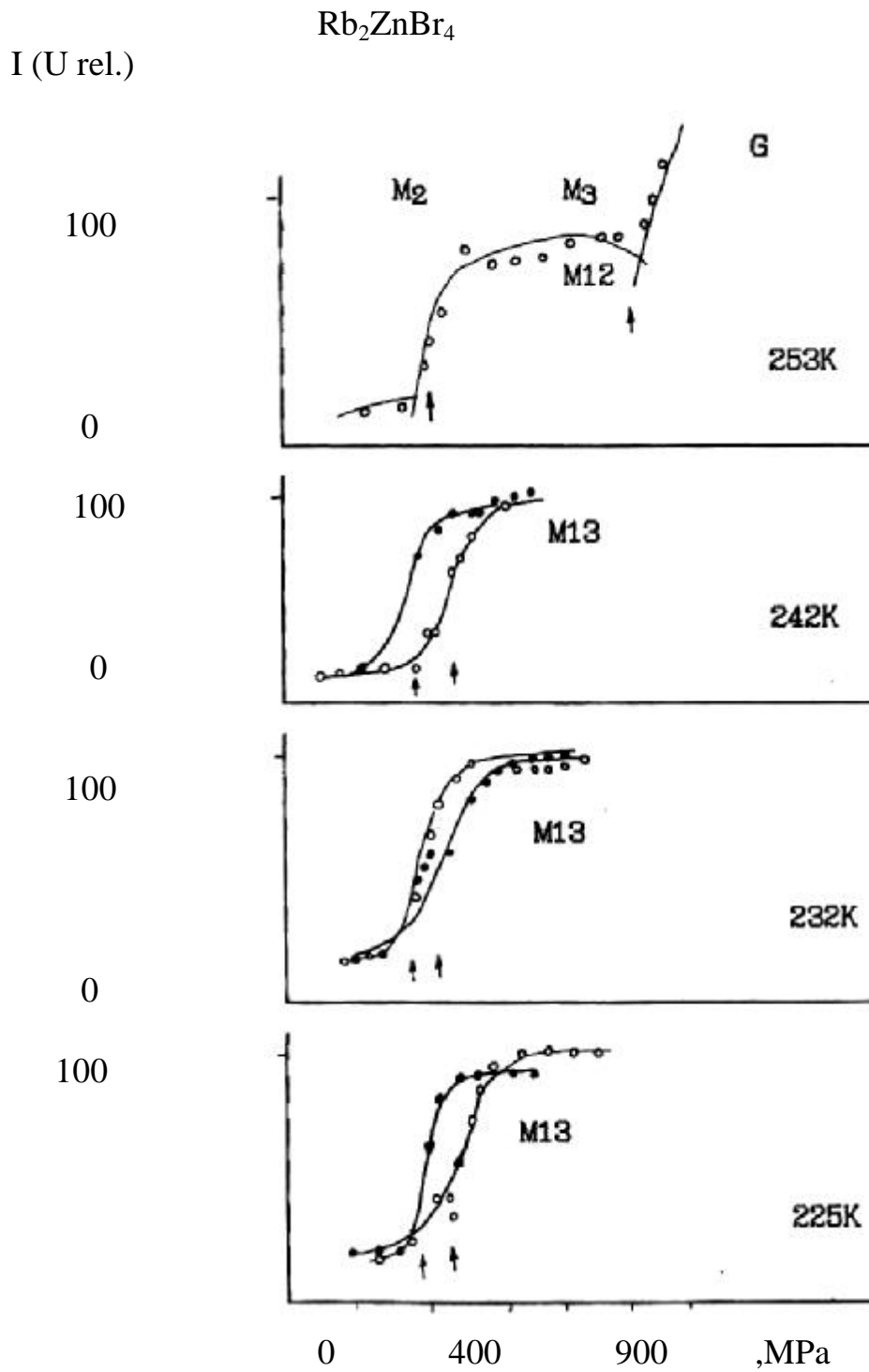


Fig.4.22. Baric of the intensity of spectral lines M13 (M12) in the phase transition  $M_2 \ll M_3$  at different temperatures.

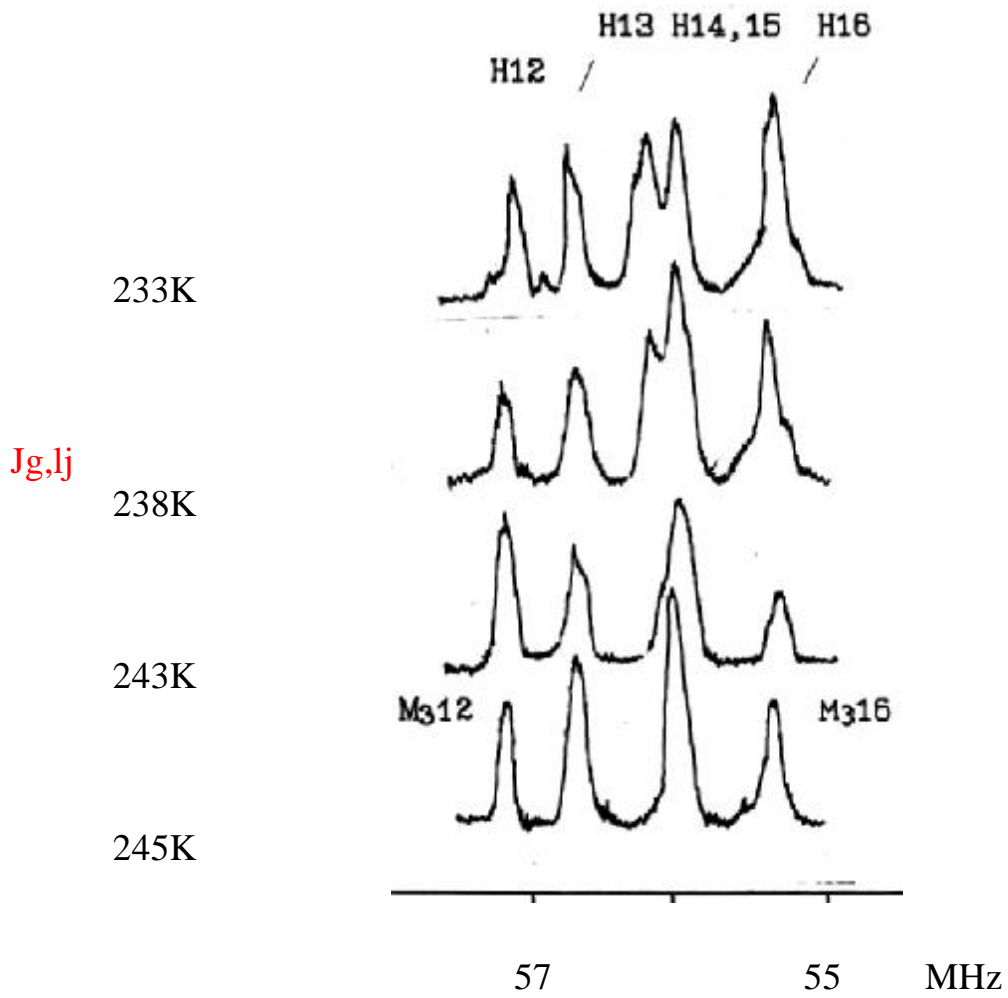
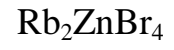


Fig.4.23. Changing of the NQR spectrum in the phase transition  $M_3 \leftarrow H$  at  $P = 500\text{MPa}$ .

Final step of transforming the structure of  $\text{Rb}_2\text{ZnBr}_4$  at high pressure is highly symmetric phase **G**, which is characterized by four powerful singlet absorption lines NQR radio nucleus BrI, BrII, BrIII and BrIV (Fig.4.18). Phase transition in phase G is a first-order transition, because, although no hysteresis phenomena (up 5MPa), there is a region of coexistence of phases. End increases with increasing temperature, and this transition is independent of the direction of change of P-T parameters.

Measurements at pressures above the transition to the 6 were not conducted.

P-T phase diagram of  $\text{Rb}_2\text{ZnBr}_4$  - On Fig.4.24 shows the experimental P-T phase diagram rubidium tetra zinc bromine in the 160-300K at pressures up to 1.0 GPa, built on the results of our data. In addition to the well-studied at atmospheric pressure paraelectric (P), incommensurate (Jc) and ferroelectric (F) phases, it was discovered or suspected the existence of several phases with different structures and symmetries.

By type and nature of changes NQR spectra investigated P-T range can be divided into two areas: 1) the area where the spectrum consists of a small number of intense singlet lines (phase F, G, F and H) and the structure of the phases described by one of the space groups simorfnyh; 2) The second area where the species and the evolution of the spectrum can be associated with the existence of more or less disordered structures (phase N, M and Jc).

Para-electric and the ferroelectric phase are known as spatial symmetry  $D_2^{16h}$  (Pnma), and  $C_2^{9v}$  ( $P2_1/n$ ), respectively. With this in mind, using the symmetry transformation rules involving data from NQR, we can show that the phase of H must have a rhombic or monoclinic symmetry. Availability 14 NQR lines, two of which have double the intensity allows unequivocally enough to suggest that this phase is described by the point group symmetry  $P2_1$  quadruple unit cell volume ( $V = 4$ ,  $Z = 16$ ). Highly symmetric phase G, which is characterized by four nonequivalent positions in structure Br nucleus may have a monoclinic or triclinic symmetry with unit relative to the paraelectric phase, the unit cell volume ( $V = 1$ ).

The latter assumption is supported by extensive, approximately 4-fold, increase in the integral intensity of each of the four NQR lines. Reduction of vernix with increasing pressure and temperature indicating the approach to a particular T-P point in the phase diagram. It also indicates the position of the P-T phase line separating Jc and P and P-Jc blur transition with increasing pressure. Based on this and several other reasons, we assumed the existence of the Lifshitz point, which should be located at the intersection of P-T lines separating highly symmetric phase G and P (Ris.4.35).

Region of existence of the disordered structure can also be divided into three parts:

1) low-temperature region N, where there is a well-defined frequency resolution and intense spectral components or groups. In this area, we can assume (with) the existence of long-period nearly commensurate structures;

2) P-T region Jc, where there are blurred spectral shape characteristic of the incommensurate phase (disordered structure of long-period);

3) Field of phases M where NQR spectra have more or less frequency resolution basis. The degree of ordering of the structure is increased when approaching the phase transitions in lines H and G phase. Reduce the blurring and hysteresis transitions between phases M1, M2, M3 with increasing pressure, also indicates the nature of the structural transformations.

P, MPa

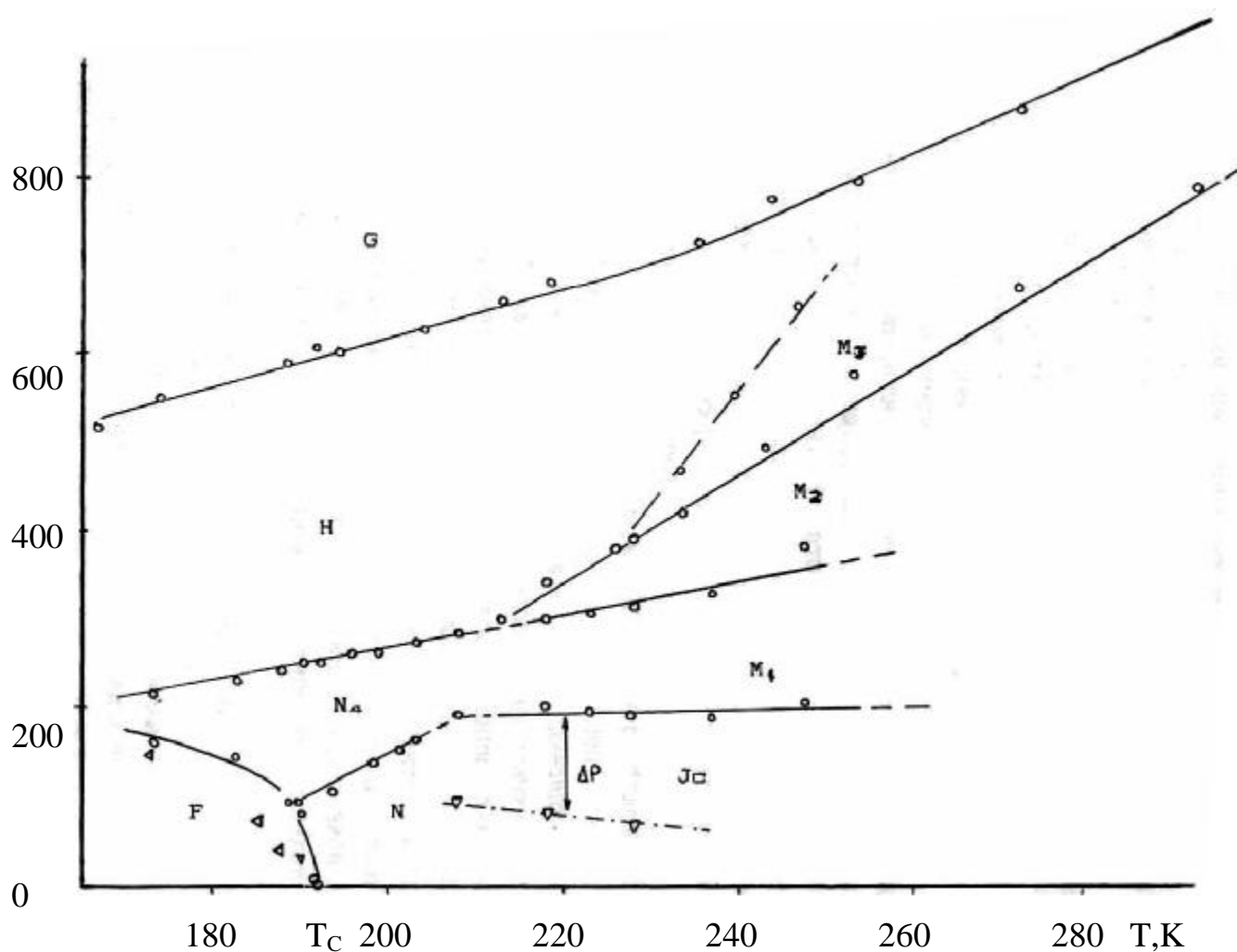


Fig. 4.24. Phase diagram of  $\text{Rb}_2\text{ZnBr}_4$ , obtained by NQR.

As in most of incommensurate phases dielectrics family  $A_2BX_4$  and in compounds with CDW [63,96] hysteresis phenomena are global in nature, and there is a large range of variation of hysteresis phenomena in different surroundings investigated P-T region, from 20 to 160MPa.

Note also feature observed in passing phase transitions  $F \ll N \ll H$  for different directions of change of P-T parameters (Chapter 4 § 2). This behavior indicates a specific data type conversions, due to the presence of significant non-equilibrium phenomena. Registers significant blurring if the transition phase as it passes along the line, compared with the transverse passage. This is apparently due to a clearer and observation of phase transitions isothermal scan compared with isobaric.

Thus as a result of these studies failed to establish the following:

- 1) With increasing hydrostatic pressure P-T transition is shifted to higher temperatures;
- 2) At pressures above 250MPa and temperatures below 220K observed commensurate phase H presumably rhombic symmetry  $P2_1$  and quadruple volume;
- 3) Has a highly symmetrical above 500MPa phase G, with the same, relative to the paraelectric phase, the unit cell volume ( $V = 1$ );
- 4) Low-temperature region of the existence of an incommensurate phase increases with increasing pressure up to 250MPa, phase transitions  $F \ll N$ ,  $N \ll H$  in isobaric mode significantly eroded;
- 5) Close  $T_C$  observed a special P-T area, increases with increasing pressure and is characterized by the coexistence of different groups of spectral lines;
- 6) In the middle region of the incommensurate phase in zoom mode pressure observed sequence of phase transitions  $Jc \textcircled{R} M_1 \textcircled{R} M_2 \textcircled{R} M_3 \textcircled{R} G$ , Apparent to transform NQR spectra.

Almost simultaneously with our studies were performed measuring the dielectric constant of RZB at different pressures [59]. Although this method is less sensitive than the NQR method, the author managed to watch some anomalies. Position of the phase transition points, tracked in this study was determined from the temperature dependence of the maxima  $\epsilon(T,P)$ , which in most cases were observed strongly blurred.

Comparison of the phase diagram Gezi (Fig.4.11) with our data shows that in the pressure 250MPa near  $T_C$ , where we tracked a special area of the phase diagram, the triple point (see details in § 4.3), by  $\epsilon$ -measurements also assumes the existence of a triple point. There is a clear coincidence P-T lines between II (Jc) and V phases Gezi and P-T line  $P_3^+$  ( $M_2 \ll M_3$ ) tracked in this study. However, other data show significant differences. First, there is no phase transition line between phases  $G \ll H$ ,  $\ll M \ll N$  and  $I \ll M_1 \ll M_2$  observed using NQR. Secondly there is the P-T phase line separating Jc in at atmospheric pressure (phase II and II' in the notation Gezi). In this case the author notes that the P-T line between phases II'-II and IV-V are fixed and not very clearly in cooling mode only, and  $\epsilon$ -peak between II(Jo) and IV phases smeared with increasing pressure. Data differences in our opinion due to the following. First, the significant influence of nonequilibrium processes, as we discovered the character structure transformation depends on the direction and rate of change of external influence. Secondly, impurities. Third, the difference polycrystal-monocrystal. It is therefore possible for a shift of the phase transition lines and their degree of fuzziness for samples of different states and crystallization.

Taking these arguments, we can explain the discrepancy between some of the data as follows. The P-T transitions between phases H  $\ll$  N, I  $\ll$  M<sub>1</sub>  $\ll$  M<sub>2</sub> is not recorded in the  $\epsilon$ -measurements due to their small inclination to the isobaric directions of measurement.

2) Mild line between phases II and II' (Gezi observed in cooling mode only), correlates with the position of P-T line P<sub>1</sub> (M<sub>1</sub>  $\ll$  Jc, recorded by us in reducing the pressure mode. The difference in the absolute position PT can be explained along with the above arguments, the difference in the determination of transition criteria.

### **§ 4.3 Features conversion spectrum near T<sub>C</sub>. Comparison with the diffraction data.**

In this section we consider in detail the change NQR spectra in the low temperature region of the incommensurate phase. As noted in § 4.2 in the P-T region of the absorption spectrum is observed, formed by the overlap of different types of spectral lines Fig.4.25, 4.29, 4.32, 4.34.

Plotting changes in peak intensities with the pressure reveals non-monotonic dependence. Presents data on Fig.4.26 typical changes in the intensities of the spectral lines with the majority of the increase in pressure, and Fig.4.27 as an example - baric moves peak intensities of lines N<sub>4</sub>, N<sub>4</sub><sup>+</sup>, close in frequency to the line F<sub>4</sub>. Well tracked fractures in galleries intensities. This behavior confirms the hypothesis based on nonsinglet lines and change their shape due to redistribution of the intensities of the different components.

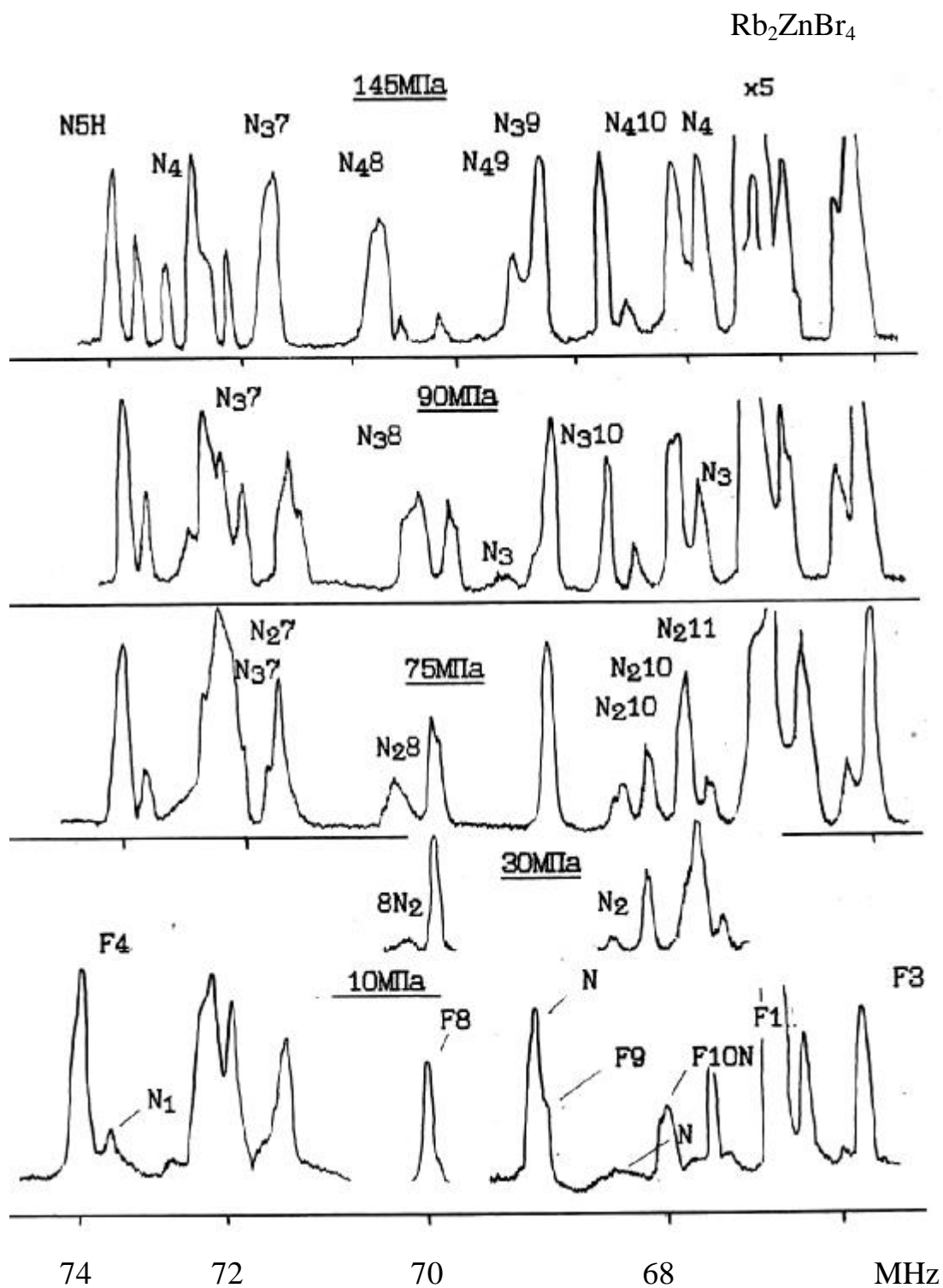


Fig.4.25. Change NQR spectrum with increasing pressure at  $T = 189\text{K}$ .

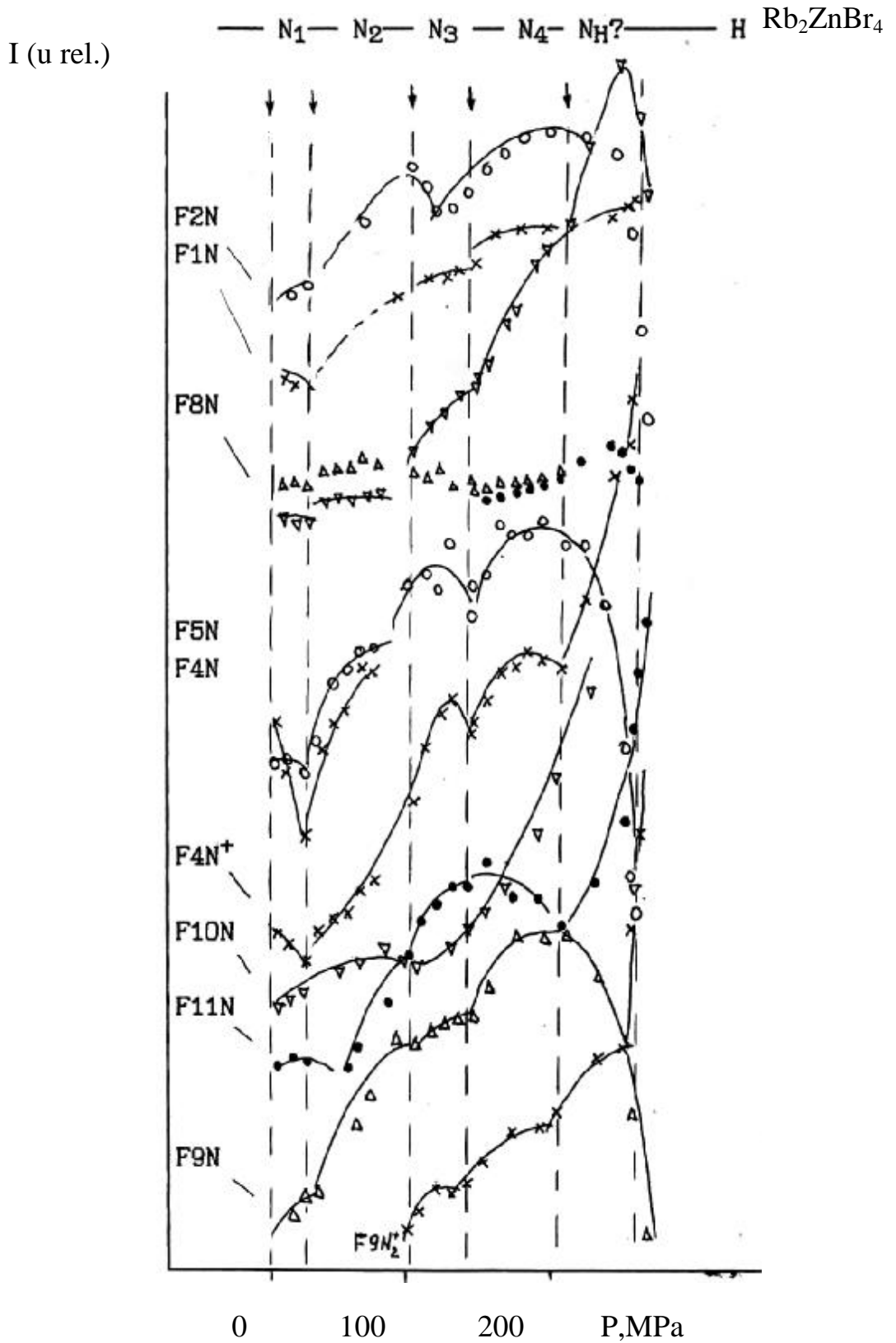


Fig.4.26. Relative change the peak intensities of spectral lines at T = 190K.

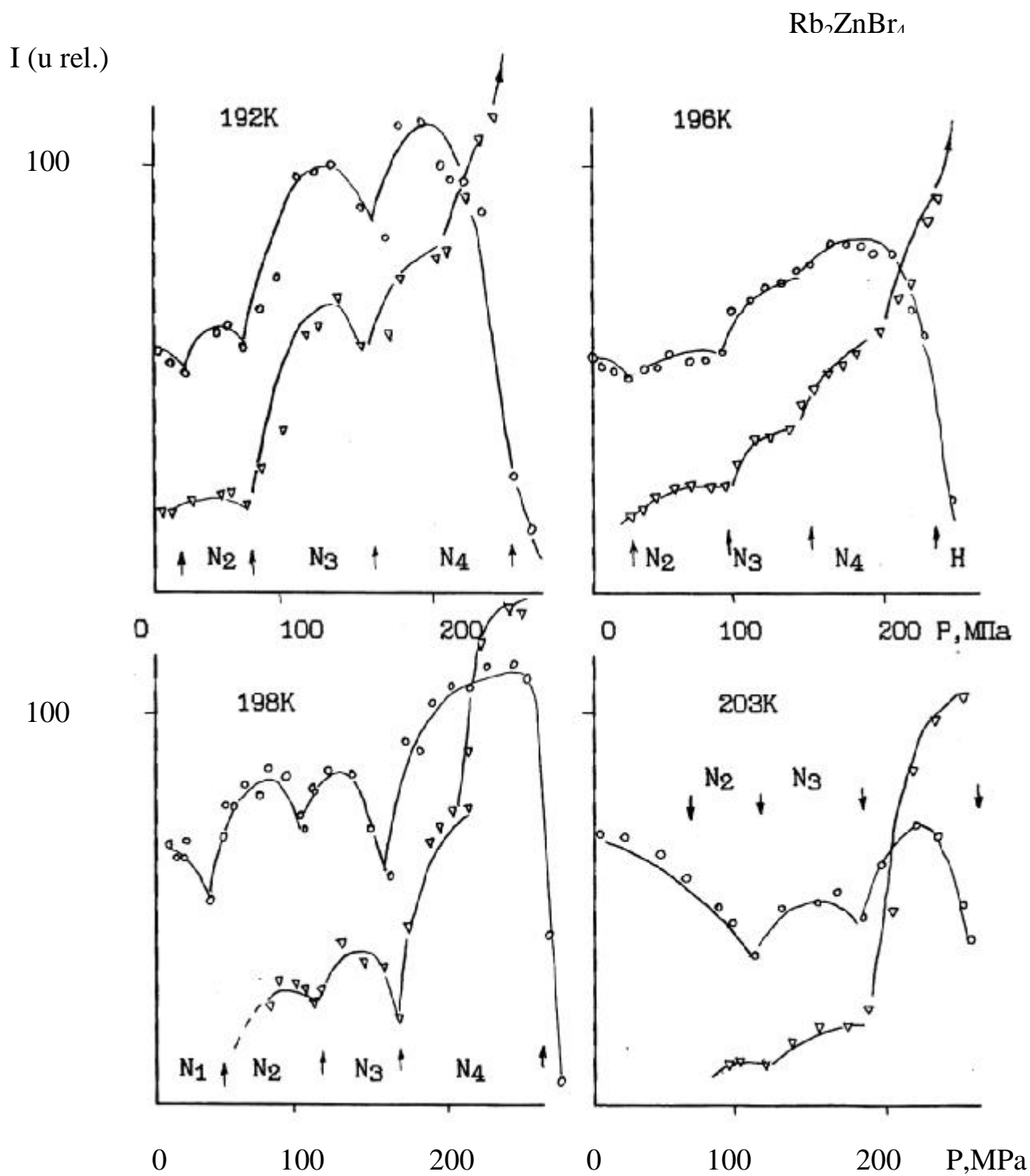


Fig.4.27. Changing the peak intensity of the spectral lines of  $N_4$  (o) and  $4 N^+$  ( $\tilde{N}$ ) at different temperatures.

Close during the specified behavior was observed intensities and isobaric studies Fig.4-5, Fig.4.12. Although the temperature scanning step was relatively large (~3-5K), but the graphs Fig.4.12, where, in contrast to [115] are all the experimental points, also noted nonmonotonic variation of intensities between Jc and F phases. Besides sensitivity of the isothermal measurements controlled NQR raper. Therefore, we are quite confident we can assume that celebrated anomalies associated with structural features, rather than instrumental errors.

Noting the arrow (on Fig.4.26 and 4.27) and symbols (for Fig.4.28) P-T conditions of the most distinct breaks and lows in the intensities of the pressure passages, we got the P-T diagram line Fig.4.28.

Turning next to the consideration of changes in the spectra observed in the PT field. With increasing pressure along different temperatures (isotherms 189, 190, 192, 195, 198 K ) in the spectrum in the process of conversion to the NQR lines, and H-type F, exhibit a number of features that can be most clearly illustrated by changing the shape of a single line on the N9\* 59 MHz frequency and Fig.4.29 Fig.4.30.

On Fig.4.29 shows the change of the line shape N9 in 190, 200K from 1 atm to 150MPa. In the upper left part of the figure in the high pressure line N9 has a well-defined asymmetric shape with two maxima of amplitude resolution. In the middle part at lower pressures asymmetry observed on the other side of the line, which is clearly seen in atmospheric changes in a heat chamber at maximum sensitivity (Fig.4.8).

Pressures above 100, 150MPa at an asymmetric location wing appears and grows on the new part of the spectrum intensity, so that at higher pressures, there is a doublet, which at the transition to H phase disappears to form a line H12. When the temperature is lowered through the N<sup>⊗</sup>F transition distribution N9 is also converted to equal intensity doublet, at a frequency of one component of which is formed ferroelectric line F9, Fig.4.30.

Analysis of the frequency redistribution of intensities within the contour line N9, assuming that it is formed by the overlap of two singlet components of varying intensity, allows present in the form of the frequency dependence of the three components (Fig.4.17).

Position P-T lines constructed by the kinks in the course of baric intensities (Fig.4.28) correlates with P-T lines separating regions of different asymmetry line N9 (Fig.4.30). The line attributed symbol (D) corresponds to the transition to the amplitude resolution of the doublet form N9.

Comparison of changes in forms of individual spectral distributions in various P-T areas also indicates that areas with identical terms of NQR structure arranged along the lines of having positive values  $\nabla P / \nabla T$ .

Model analysis of the full range of NQR is beyond the scope of this work. However, we try to make an initial discussion. Isothermal passages in HPC2 at low pressures showed that the phase transition Jc general form of the spectrum in a very narrow neighborhood before  $T_C$  (2, 3K, 3K 60MPa) differs from atmospheric pressure. Along with the NQR lines of type N, recorded at atmospheric pressure (which we assigned here, the index  $N_1$ ), other-marked line, which we denote the index  $N_2$  Fig.4.32. Changing forms of spectral distributions can be represented by the assumption that near each of the 12 lines of type F, close to the frequencies is a few lines of type  $N_1$  and  $N_2$ . With increasing pressure, the intensity of the lines of  $N_2$  increases, and the line intensities of the  $N_2$ , within certain limits

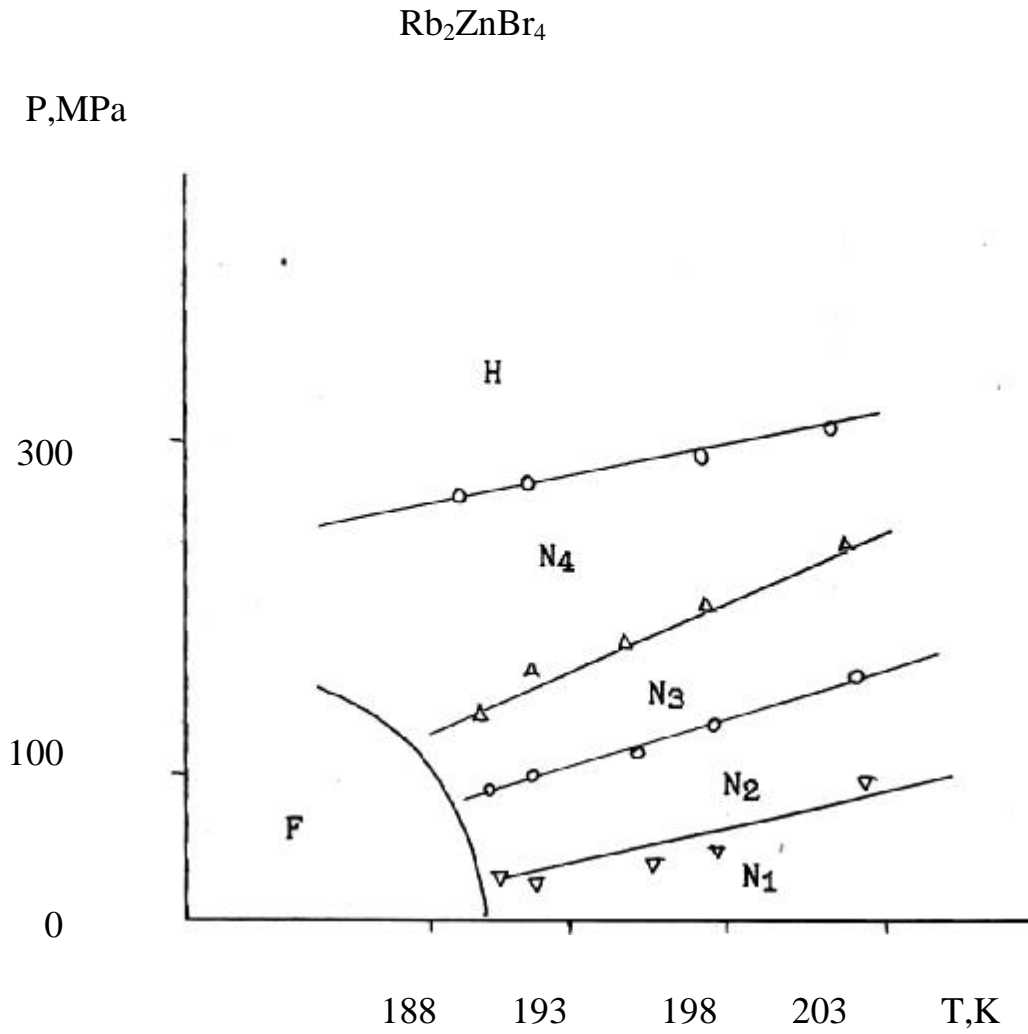


Fig.  $P$ - $T$  field  $J_c$  phase near  $T_C$  marked by anomalous change of the line intensities of the NQR spectrum.

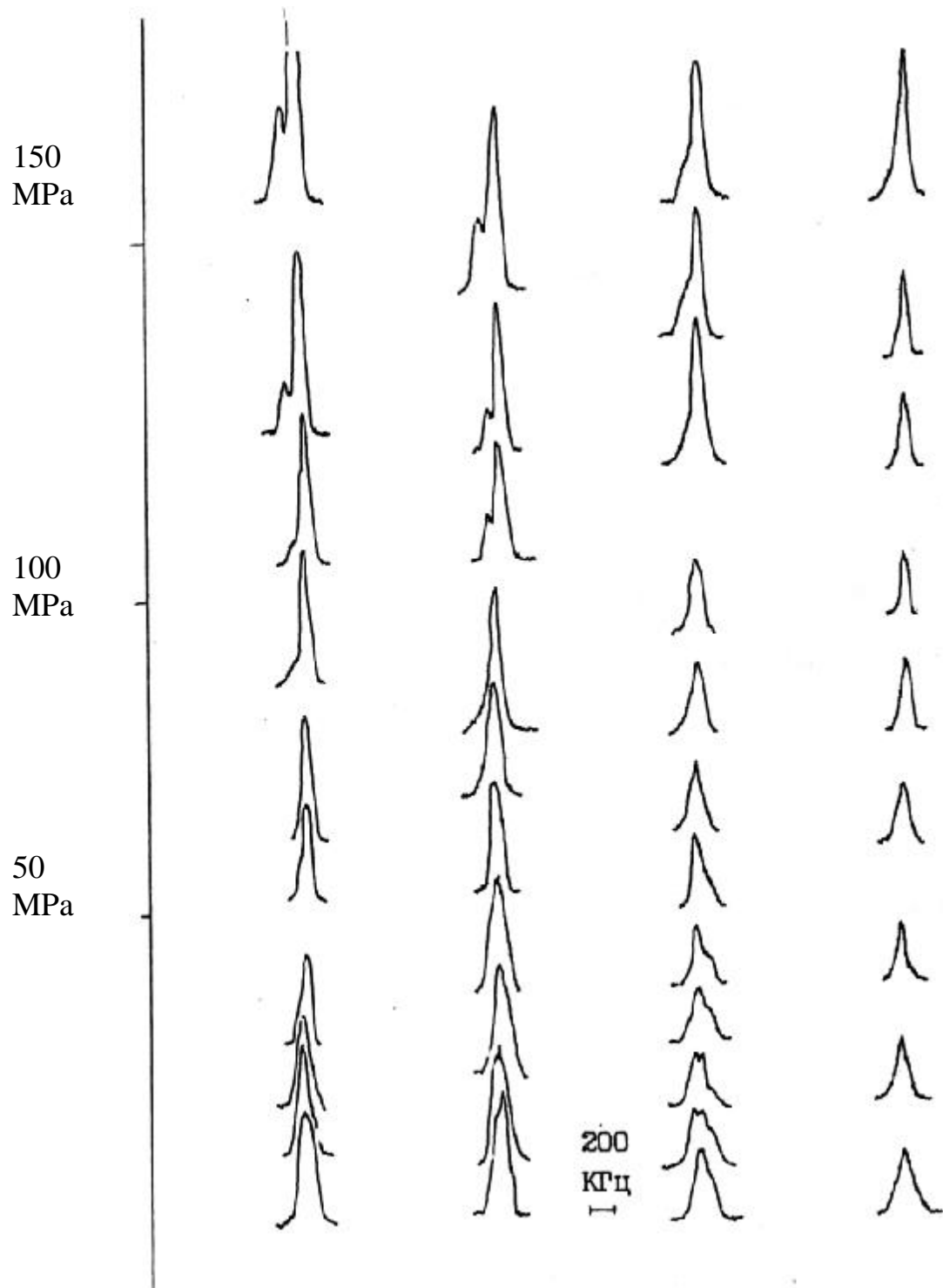


Fig. Variation of the spectral line shapes of type F9-N9 near  $T_c$ .

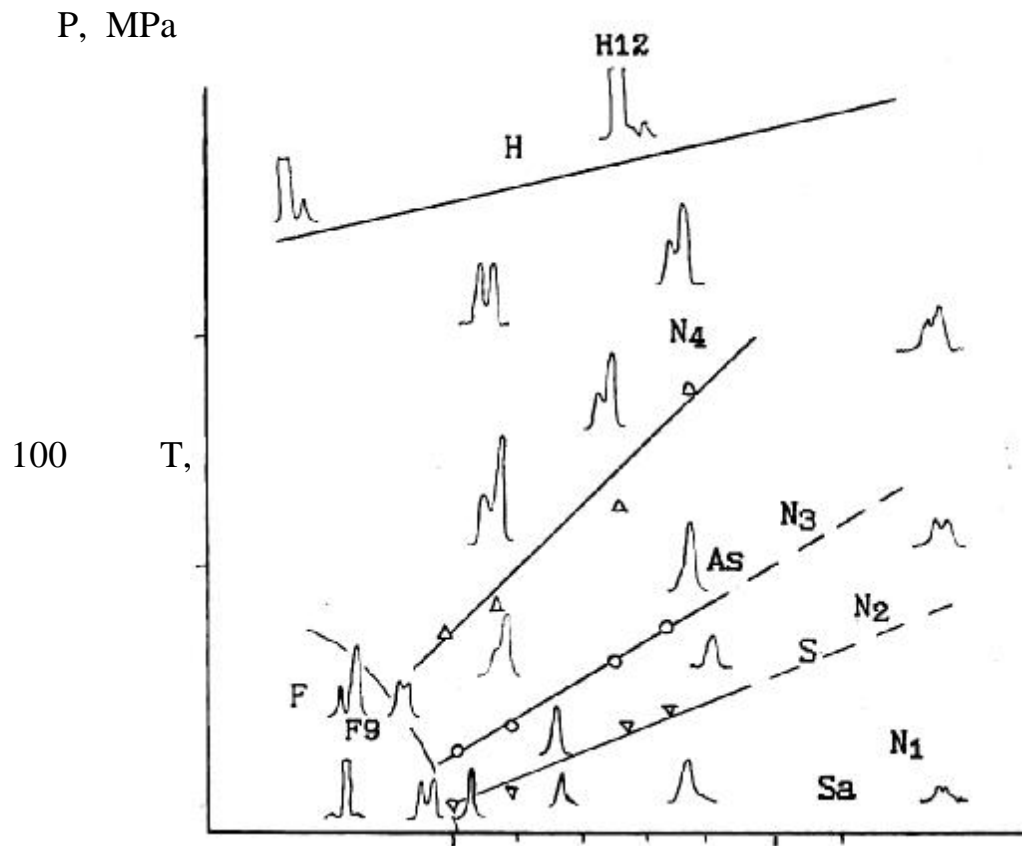
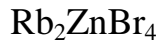


Fig.4.30. P-T field with varying degrees of asymmetry in the line F9-N9-H12.

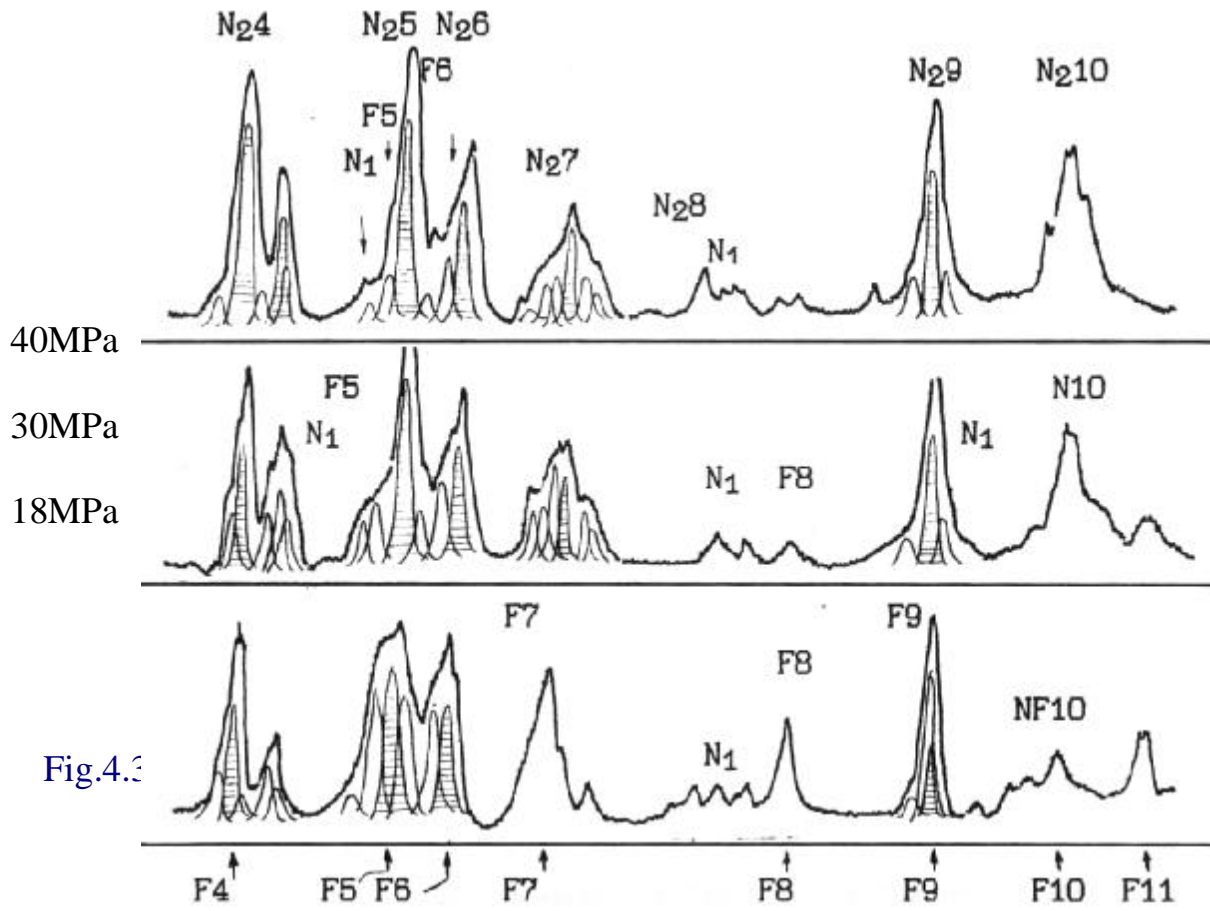
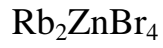


Fig.4.3

spheric

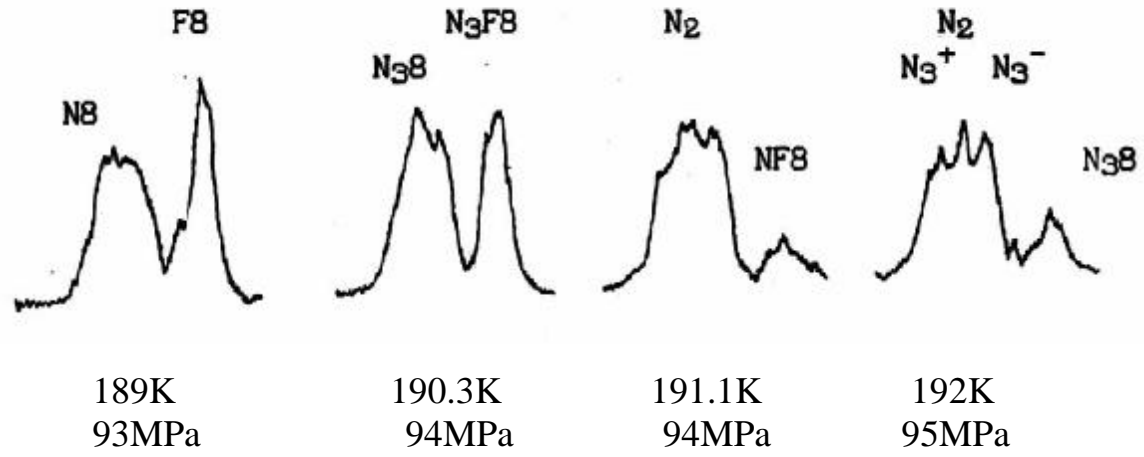
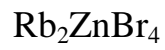


Fig.4.33. Change line NQR spectrum N9-F9 when the temperature changes. P = 100MPa.

vary slightly. Some of the lines are close in frequency, and the peak intensity of the course in this case should be determined by the different contributions.

A similar redistribution of the intensities observed at the transition to the regime of heating in the pressure 100MPa, Fig.4.33. In this case, the change can be represented by overlapping the three groups of spectral lines, as illustrated in Fig.4.33 for the spectral distribution FN8.

At temperatures above  $T_C$ , where the NQR lines of the phase F is absent, the spectrum at low pressures presented overlapping lines of type  $N_1$  and  $N_2$ , Fig.4.34 (a-h).

As the pressure increases in N above 80~150MPa range transformed to Fig.4.25d Fig.4.34i-r. His change can be interpreted as the appearance within the contours of spectral distributions of new lines of type  $N_4$ . Characteristic features of the changes are: a) design of asymmetric line wing  $N_9$  ( $\nu=68,98$  MHz), b) the emergence of low-intensity lines  $N_3^+8$ , in characteristics redistribution of intensities of lines in the group  $N_5$ - $N_7$  and  $N_{10}$ - $N_{12}$ , etc. Then in the world designated as  $N_3$  shape of the spectrum with respect to stable.

Pressures above 110-200MPa, where there is a third anomaly during the peak intensities, also notes changes in the spectrum. Asymmetric line wing  $N_9$  is made in a separate spectral component  $N_4^{+9er}$ . Change appreciably other spectral distribution (Fig.4.34s-h). The above P-T line separating the region of the  $N_3$  region designated by us as  $N_4$ , a broad range of P-T interval is (Fig.4.34s-h).

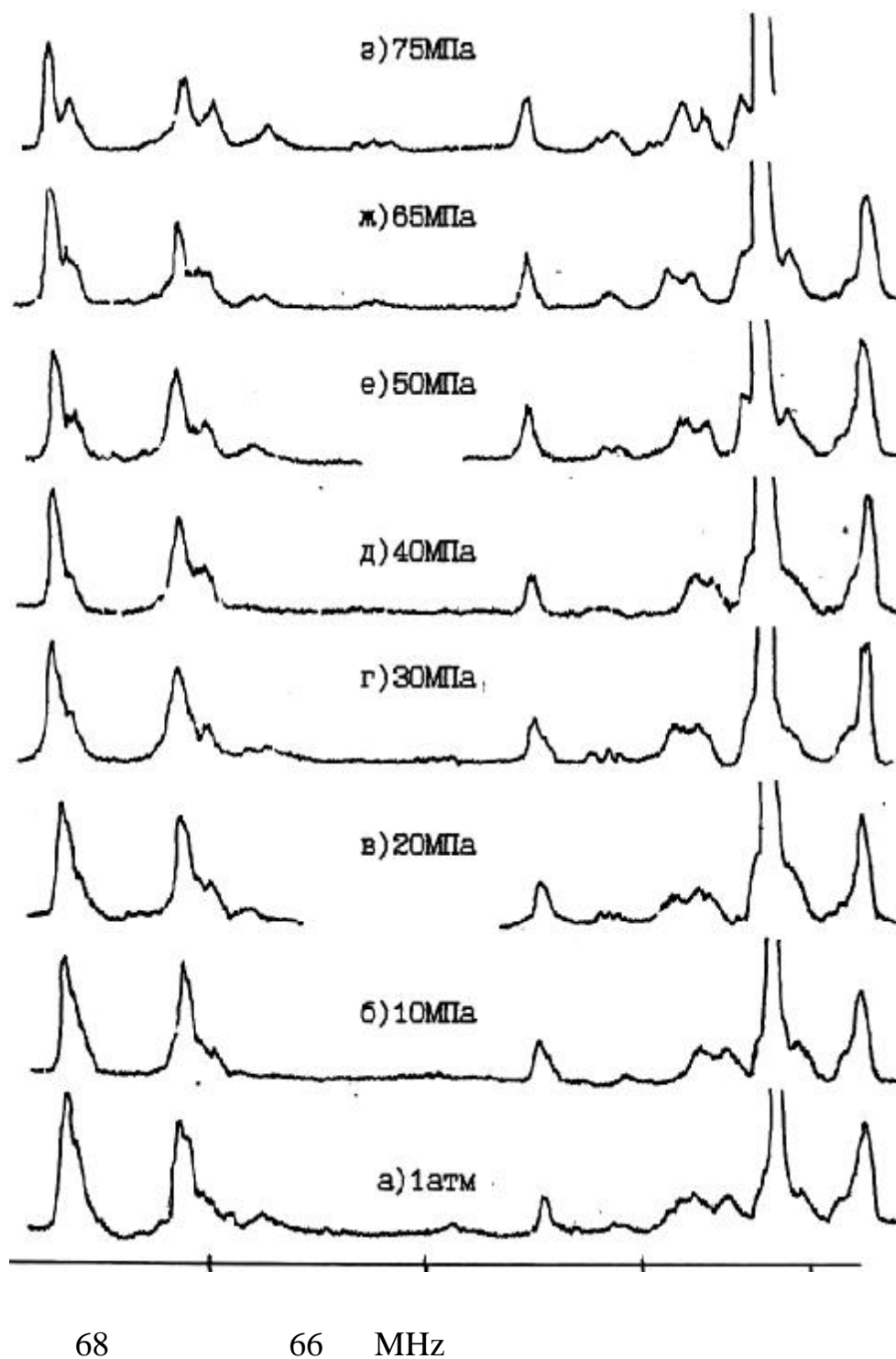
The slope of the pressure stroke frequency of certain lines (Fig.4.19). Higher pressures ( $> 250$ MPa) phase transition is observed in the phase of H (see § 4.2) tracked the fine structure of the NQR spectrum and notes anomalies in its change in the temperature range 190--210K it possible to identify the P-T phase diagram of  $N_1$ ,  $N_2$ ,  $N_3$ ,  $N_4$ , we (in the framework of the "devil" and the stairs in accordance with the data of X-ray diffraction) was interpreted as a manifestation of stages or phases D'Starcase high-order symmetry (HOS) [113,114], and the lines near phase transitions in the area of triple points observed at the coexistence of at least two or three adjacent phases. The magnitude of the coexistence region (shaded region Fig.4.35) and the number of phases is determined by the direction of change of P-T parameters and degree of symmetry.

In  $(NH_4)_2ZnCl_4$  and  $(NH_4)_2ZnJ_4$  where change was observed in the multiplicity of NQR spectra from 16 to 12 absorption lines with narrow temperature intermediate phase, X-ray diffraction at atmospheric pressure are also recorded sequence  $Jc - 1/4 - 2/7 - 1/3$  [47], Figure 1.6, Table 4.1 (p.158).

Interpretation of the data presented NQR was quantitatively tested on samples of  $Rb_2ZnBr_4$  of the same series of crystallization On the basis of the reactor international scientific center of Orsay (France), measurements were made of the position of the wave vector  $q_d$  in P-T region of its evolution in F and H phase method by neutron diffraction [119].

Interpretation of neutron data at atmospheric pressure X-ray diffraction data does not contradict the study [110] about the existence of near  $Jc$  values  $q_d$ , which may be

Rb<sub>2</sub>ZnBr<sub>4</sub>



70 68 66 MHz

Fig.4.34. Detailed change in the total NQR spectrum at T = 194K and pressures from 1 atm to 75 MPa.

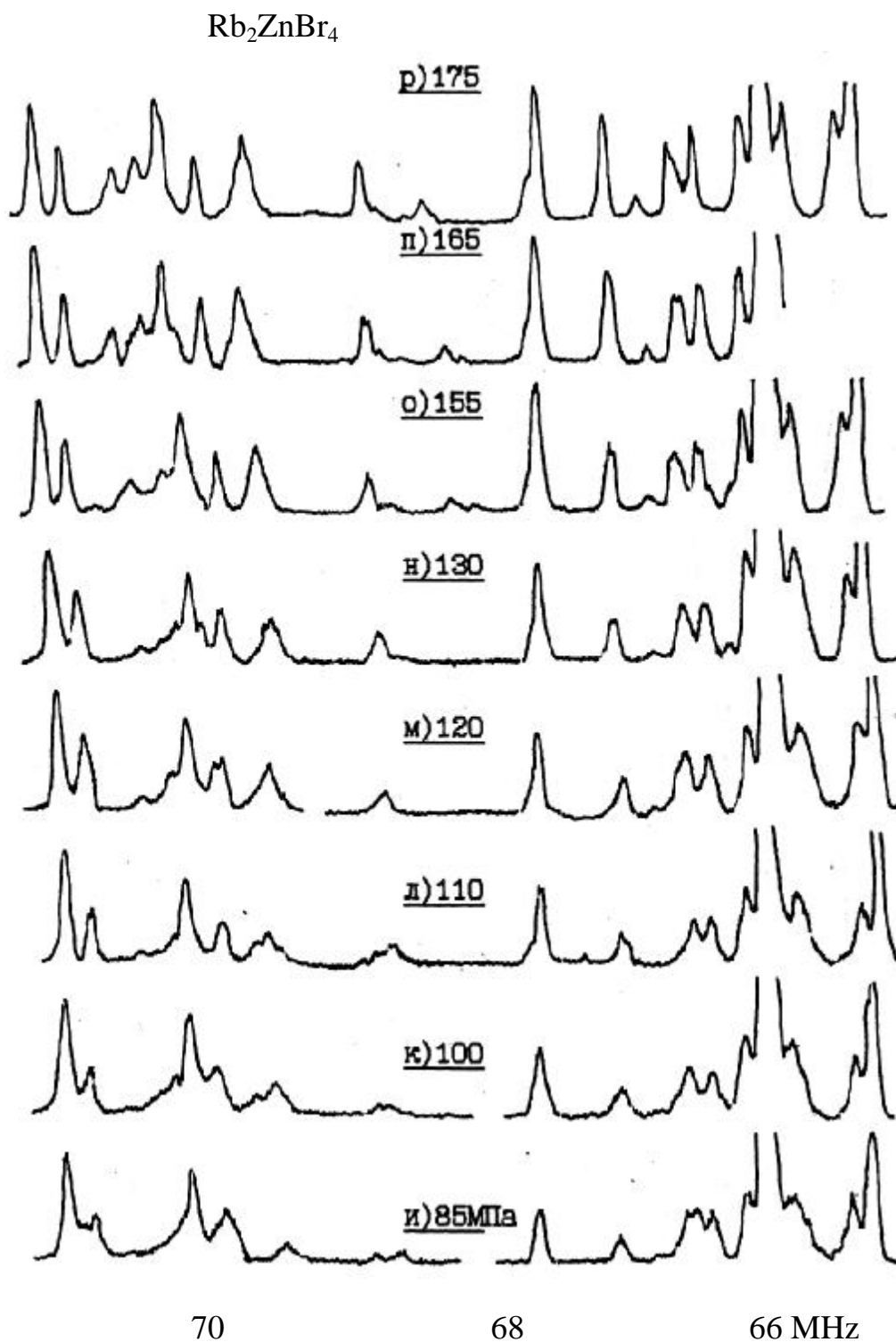


Fig.4.34 (и-п) Detailed change in the total NQR spectrum at  $T = 194\text{K}$  and pressures from 85 to 175 MPa.

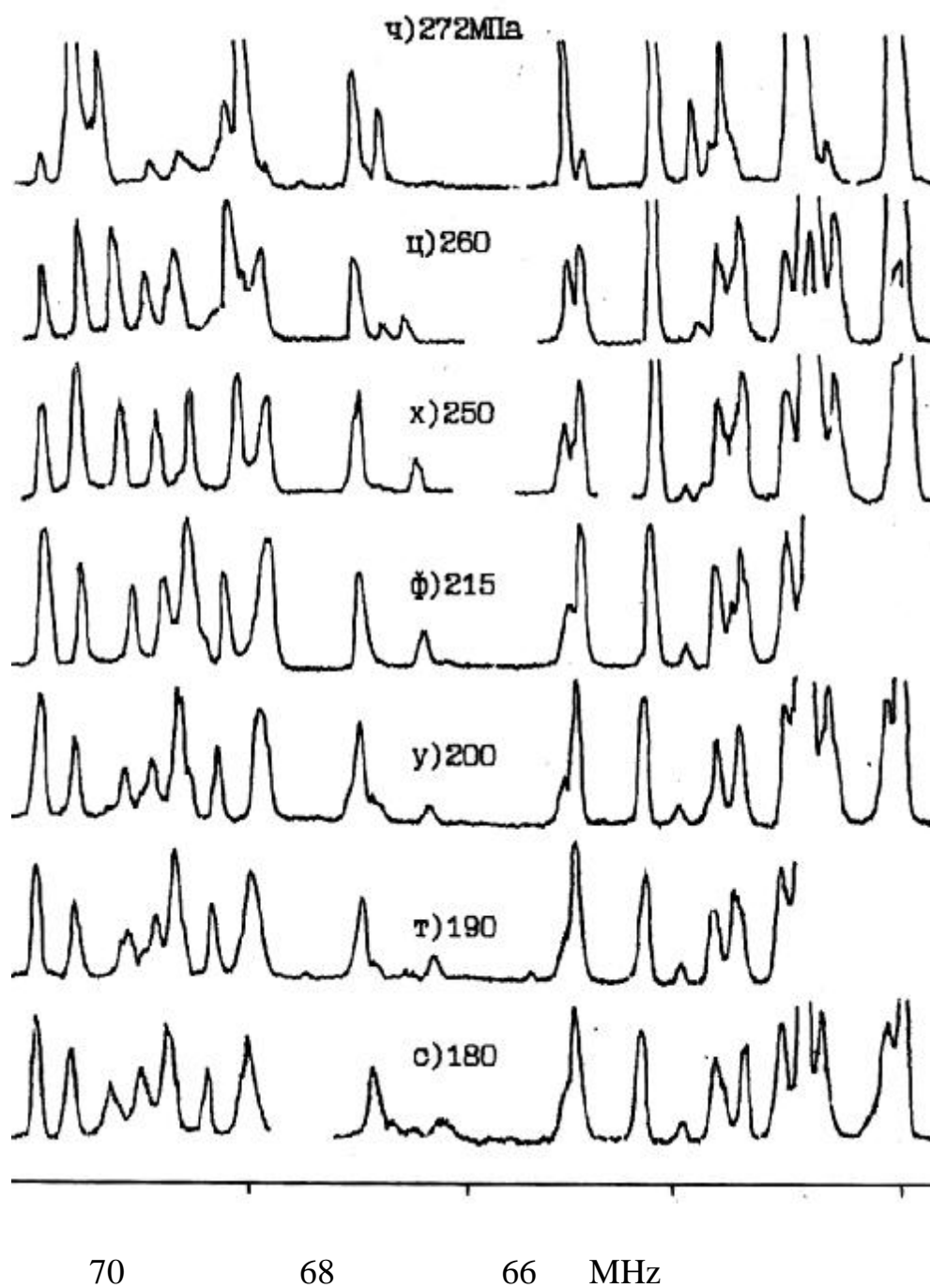
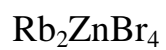


Fig.4.34. Detailed change in the total NQR spectrum at  $T = 194\text{K}$  and pressures from 185 to 300 MPa

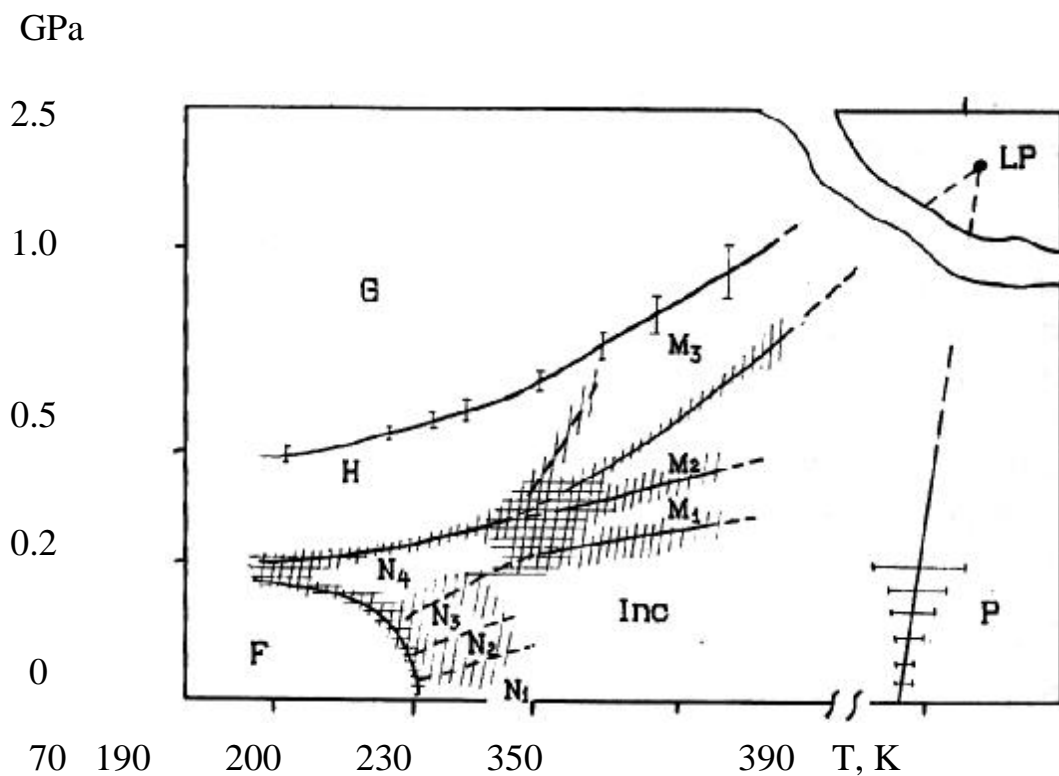


Fig.4.35. General view of the phase diagram of  $\text{Rb}_2\text{ZnBr}_4$  according NQR Br.

conventionally disposed at steps "going up" ladder:  $5/17 \textcircled{R}$   $3/10 \textcircled{R}$   $7/23 \textcircled{R}$   $4/13 \textcircled{R}$   $5/16 \textcircled{R}$   $1/3$  (in the unit.  $\mathbf{a}^*$ ).

With increasing pressure, has been confirmed, detected previously [115], lock-in the phase transition orthorhombic symmetry  $Pn2_1a$ , with a cell volume quadrupling ( $Z = 16$ ) with the value of  $q_d = 1/4$  (0.2500). While additionally observed values  $q_d = 0.296, 0.2917, 0.2857$ , missing at atmospheric pressure. These values  $q_d$  authors of [119], following we [113] compared stairs going down stairs:  $3/10, 8/27, 5/17, 7/24, 2/7, 1/4$ . In this region of the incommensurate phase was marked by the coexistence of two or three satellites in Jc phase diagram. (Satellites  $1/3$  (0.3329)  $5/16$  (0.3114)  $5/17$  (0.2948)  $7/23$  (0.3043)  $7/24$  (0.2917), Fig.4.36). At the same time, according to data NQR noted preferential coexistence of three satellites at isobaric aisles near  $T_c$  and two satellites under isothermal. Also large widths were fixed caliper with cooling, and the continuous change in the position, especially at low pressures. However, the scattering profiles were slightly different from the X-ray [51], a smaller width and temperature region of coexistence. Slightly different conditions and observations: for neutrons pressure was about 1 kb, and X-rays at atmospheric pressure. According to such an NQR contrast at low pressures from outside the structure indicates difference at atmospheric pressure of 1atm under the atmospheric 1tm at  $T_c$ . In the middle part of the incommensurate phase observed continuous decrease in the magnitude of the wave vector  $q_d$  with increasing pressure (from 0.293 to 0.28 at  $T = 273K, P < 300MPa$ ) and a slight increase in  $q_d$  at low temperatures (from 0.2017 ( $5/17$ ) to 0.300 with  $P \gg 1.0 MPa, 273 < T < 200K$ ). According to the measurement of NQR and neutron diffraction authors [119] was constructed P-T phase diagram (Fig.4.37), which is well distinguished from the proportionate phase wave vectors of  $1/3$  and  $1/4$  and the region with the higher order phases. The phase transition between phases  $1/3 \ll HOP$  and  $HOP \ll 1/4$  exactly coincide with the P-T lines between phases  $F \ll N$  and  $N \ll H$  fixed NQR. In the HOP, where there is a coexistence of satellites, proposed a hypothetical phase diagram presented a set of conventionally separated pseudo incommensurate structures. However, according to another inclination NQR observed, compared with the data NQR P-T lines, separating regions of high phase order.

P, kb

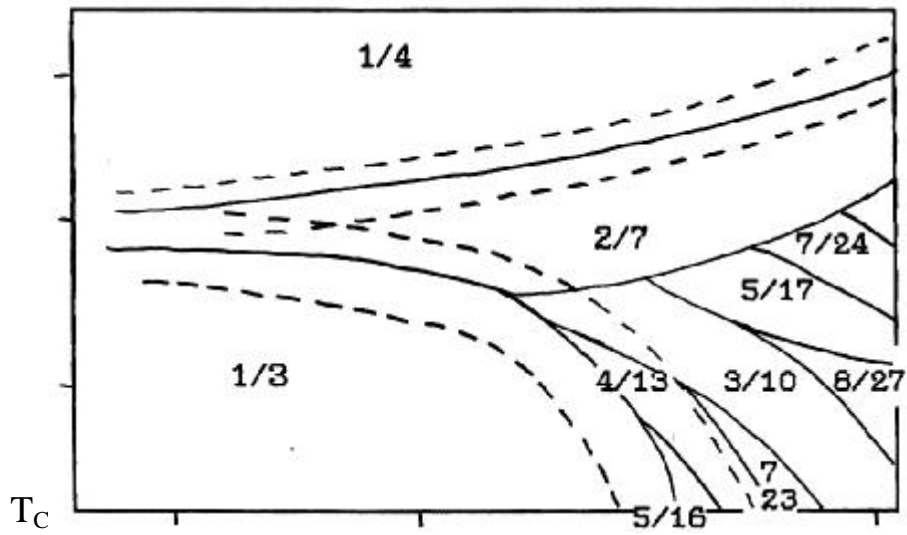


Fig. A phase diagram of  $\text{Rb}_2\text{ZnBr}_4$  near  $T_C$  of analysis neutron diffraction data.

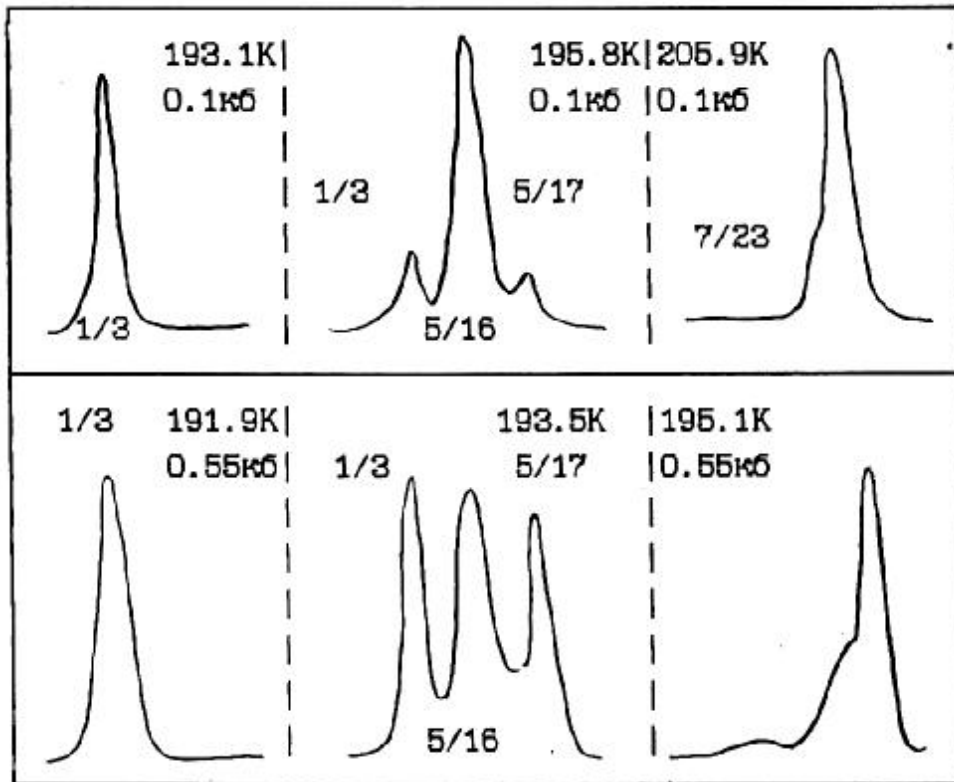
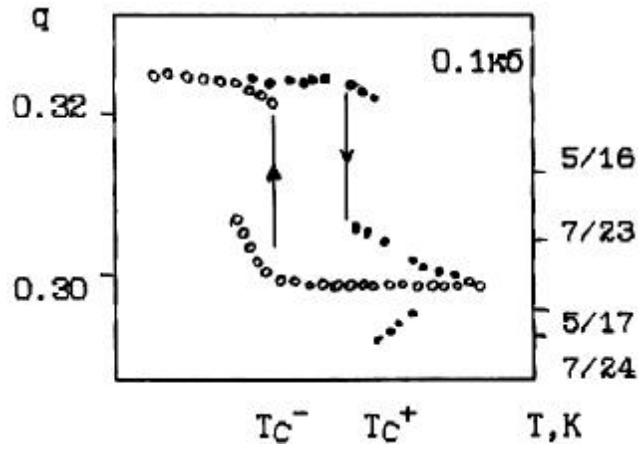


Fig. Scattering profiles and repositioning the satellites according neutron diffraction scattering.

## § 4.4 Discussion of the phase diagrams in the framework of theoretical models "devil's staircase".

In conclusion, we provide a synthesis of the experimental P-T diagram of  $\text{Rb}_2\text{ZnBr}_4$  according NQR (Fig.4.35) and compare it with the theoretical phase diagrams obtained by numerical methods. Calculations performed in [15,12,121] are based on the anisotropic Ising model with the interaction up to three neighbors. We are interested in that part of the phase diagram, where realized structure with a period close to  $1/3$  and  $1/4$  Fig.4.38a. In this diagram, the value of  $q_d = 1/3$  corresponds to the configuration of spins  $\langle 12 \rangle$  (one up, two down),  $q_d = 1/4$ -  $\langle 121 \rangle$ ,  $q_d = 5/17$ -  $\langle 1121212 (12) 2 \rangle$ ;  $2 \rangle$ ;  $q_d = 3/10$ -  $\langle 112 (12) 2 \rangle$ ; etc. If this diagram spend dashed line, as shown on Fig.4.38a, and relate it to the experimental scale temperature at atmospheric pressure, is located above this line, the phase diagram [121], would be enough comparable to the experimental P-T diagram obtained world. In this case the transition to the modification of this model in the framework of the pseudo-spin variables [12], the region of existence of structures with different configurations can be changed (Fig.4.38b).

A somewhat different approach developed in recent years [12]. Its foundations were laid by a modification of the parabolic model of Frenkel-Cantor and put nesimorfny symmetry element, which acts as a nonlinear part of the polarization of communication between sublattices. With the increase of the contribution of the nonlinear polarization  $P_{NL}$ , in a structure with symmetry series  $Pnma$ , phase fractions of  $1/3$  and  $1/4$  respectively decrease and increase, appear between lower-order symmetry structures (Fig.4.39). Inset on a larger part of the diagram shows Fig.4.39 Aubrey, which can be compared with our P-T phase diagram.

When considering the field of existence of the phase  $2/7$ , located between phases  $1/3$ ",  $1/4$ " phase diagram Aubrey and lines separating phases  $1/3$ ",  $1/3$  and  $5/17$ , we can imagine that in our case there a fine structure of these regions (as shown in Fig.4.39b) as intermediate steps between  $1/3$  and  $5/17$ , and between  $5/17$  and  $2/7$ . In this case, the phase diagram obtained RZB NQR based on the values of the wave vectors of the measured diffraction neutron diffraction well compared with the theoretical phase diagram in the model Aubrey [12].

As follows from numerous data on the experimental study of the phase diagrams of various systems with frustrating interactions diagrams complication occurs not only in the case of registration of more distant neighbors across the anisotropy axis of the system, but with the introduction of structural disorder (random field). The latter may be due to impurities,  $\text{H}_2$  bonds, nuclear isotopes, as well as presence in the crystal layers or surface phases of another structure. Omitting, however, the discussion neutron diffraction [124, 21] and scaling [123] type of behavior that can be observed in this case, we dwell on the reasons leading to the stochastic regime celebrated applications of three-dimensional and two-ANNNI models [13]. If, for example, the energy of the system is close to the case of a tripling of the unit cell (or  $j \approx \pi/3$ ), the average structure is a topological articulation solitons, antisolitons and their random combination. Depending on the interaction, some combinations will be energetically more favorable. Such chaotic phase will be metastable, and the degree of metastability depends on the communication parameter disproportion to the elastic energy. Infinite (or finite) number of stable states of a set of "devil staircase"

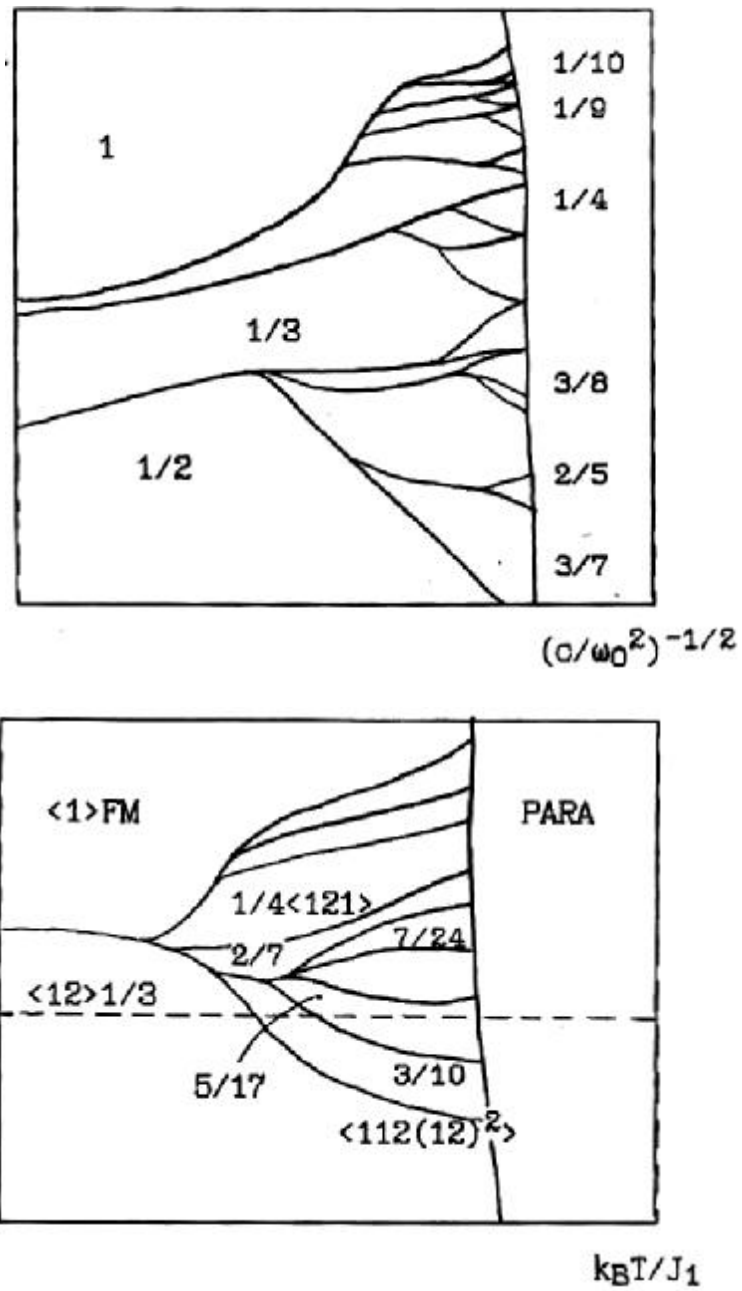


Fig.4.38.  
 a) theoretical diagram Celka [121];  
 b) phase diagram Aubrey [5].

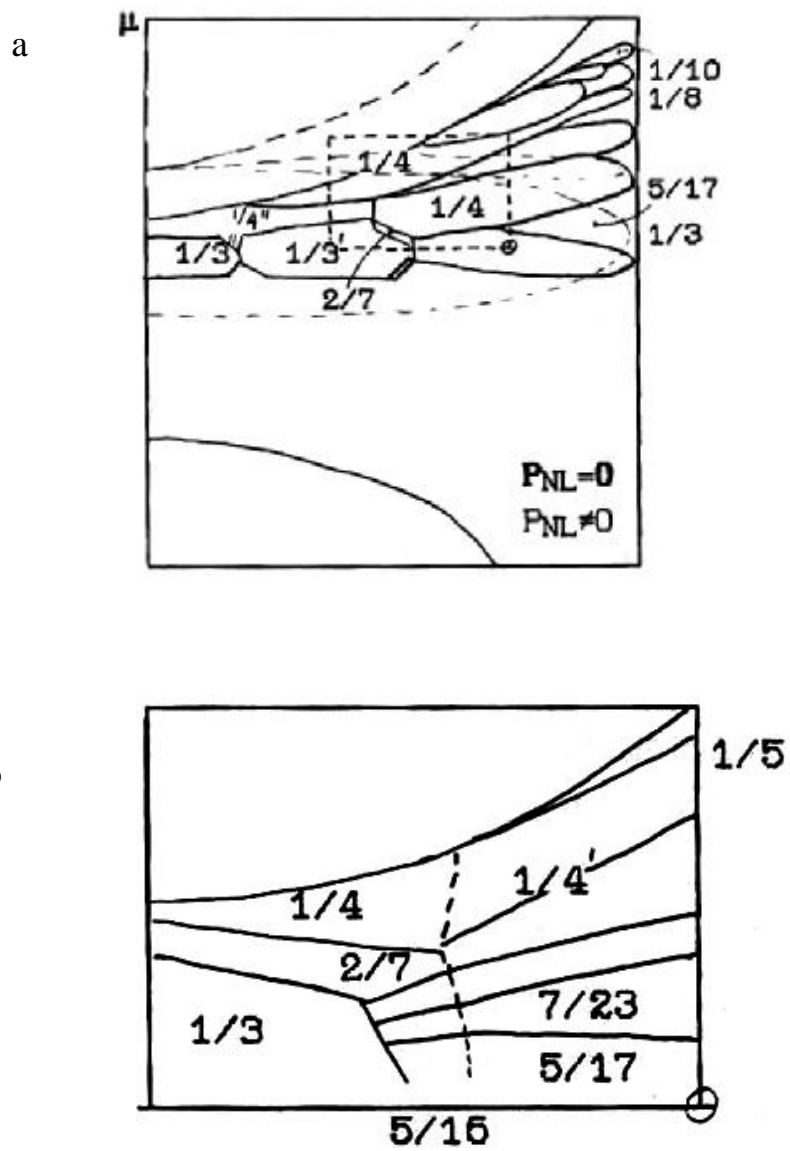


Fig.4.39. Theoretical phase diagram of the polarization model Aubry [12].

can be separated by energy barriers and the real system can not relax to the ground state in a finite time.

In this mode, there are two cases: weak and strong interaction potential [13,120]. In this case, when the distance between solitons small incommensurate phase is stable. When the distance between the solitons, repulsive interaction between them can not overcome the pinning lattice and observed soft chaotic regime. With significant excess disproportionate period compared with the lattice period, high-temperature phase is stabilized. Here it is possible to conduct a similar cluster pretransition ordering.

At strengthening ties between the sublattices ANNNI model (strong potential), the width of the chaotic regime can greatly increase and the incommensurate phase will be able to include some long-period phases. For example, instead of the phase  $q = 2p/4*(1-q_d)$  in the range of wave vector  $q \pm Dq$  four possible modulation states  $q = 3/16 = 1/4*(1-1/4)$ . The phases will differ phase shift value  $j = j_0 \pm Dj$  close to  $p/4$ . When these four long-period would be two chaotic phase. When reducing the magnitude of the wave vector number energetically close phase will increase. Each incommensurate phase is represented by a set of long-period and chaotic phases. In this case, should be observed smoothed (incomplete) mode «Devil's staircase», as opposed to purely chaotic regime, where the wave vector varies according to the classical (smooth) mode Devil's staircase'. In this case (for large values of the period disparity) is true incommensurate phase is not realized.

To analyze this possibility in our case, we, on the [120], should appeal to the structure of Pnma. As is known, the structure of  $A_2BX_4$  type  $\beta$ - $K_2SO_4$  in a certain layer ab-plane of the two centers of gravity  $BX_4$  tetrahedra are located at the same level as the ion A (Fig.3.14). Between coats  $z = 1/4$  and  $z = 3/4$  A ions are remaining. When considering the structure within a single layer, it can be assumed that the electrostatic force acting within the layer is not stable, whereby there is the rotational mode, which each tetrahedron rotates so that the other two in this tetrahedron unit cell are rotated in opposite directions. Structure should stabilize spatial redistribution of the charge between the ion A and one of the X atoms of the tetrahedron. Potential energy within the layer can be represented by a double pit: a polynomial of fourth degree of  $j$ . Interaction between the layers appear in the repulsion between the top and the base of the tetrahedron tetrahedron lying in another layer, and through A ions. When along the c direction has two layers on the lattice constant (such as in  $Rb_2ZnBr_4$ ), the potential energy of interaction of ions can be characterized by the rotation of the pyramid in the n-th layer at an angle  $j_n$  and is represented in form similar to  $j^4$  discrete tasks ANNNI model [120]:

$$V = \mathring{a} | A/2 \times \varphi_n^2 + 1/4 \times \varphi_n^4 + B \times \varphi_n \varphi_{n-1} + D \times \varphi_n \varphi_{n-2} |$$

As is known, in this case there are non-linear solutions (Eg "solitons"). For the calculation of the parameters **A**, **B** and **D** need to know the specifics of the interatomic interactions and the structure of the chemical bond. However, some solutions  $j^4$  models have a chaotic regime. As shown in [120,122], in particular cases, for small values of width **1** "solitons" relative lattice constant (narrow solitons), there are several states with high-order proportionality little distance between solitons  $l_0$ . With an increase  $l_0$  and reaching its value a certain critical value  $l_{cr}$ , a mixed state becomes chaotic behavior with randomly pinned (anti) solitons.

Trying to satisfy neutron diffraction data, X-ray scattering data and RF, we can represent the structure of the incommensurate phase of an infinite set of fragments with a long

period, which differ in the non-equivalence of the chemical bond in subfragment located in the structural cell in a certain way. For example, assuming that N<sub>4</sub> phase, Rb<sub>2</sub>ZnBr<sub>4</sub> crystal cell 14 has a size of the lattice constant, the substructure it can be composed of two fragments with a length **3a<sub>0</sub>** and **4a<sub>0</sub>** of the two in the lattice constants relative to each other spaced randomly (mixed nonlinear solutions). In the primitive description limited fourteen tetrahedra (in their double-well Librational position), we can make a subcell **3a<sub>0</sub>**, for example, one of the tetrahedron in the left and two in the right position, and **4a<sub>0</sub>** subcell of the two left and two right successive tetrahedra. Then cell 14**a<sub>0</sub>** can be represented on five ways (basic solutions) consistent position two nested cells **3a<sub>0</sub>** and **4a<sub>0</sub>** two cells. One of these methods may be more favorable. In the full sense of the overall structure is determined by the specific nonlinear solution.

Spreading such structuring on the high temperature region of Rb<sub>2</sub>ZnBr<sub>4</sub>, one can try to describe the transition structure of the 5/17 to 1/3 or 1/4 for each halogen atom tetrahedron through a small redistribution of electron density in a group of neighboring atoms (flash polarization). In implementing such a process cell size is reduced through a series of steps to **3a<sub>0</sub>** or **4a<sub>0</sub>**. Modulation does not seem continuous displacement of nucleus from state to state, and the redistribution of the electron density of the two ranked energetically close structures **3a<sub>0</sub>** and **4a<sub>0</sub>**.

According to this concept, according to NQR Rb<sub>2</sub>ZnBr<sub>4</sub> under pressure in a wide temperature range from T<sub>i</sub> to 230K near atmospheric pressure observed mixed mode and a long-chaotic behavior. This is evident from a comparison of the observed shape of the spectrum, which is directly after annealing presented blurred frequency distributions. In this case, the diffraction data, where there is a blurred satellite in the same position ( $\approx 5/17$ ), see only the periodicity of the structure. At T<sub>c</sub> phase transition to a long-F behavior prevails over chaotic. And with increasing pressure to phase H, the chaotic behavior is almost completely disappears and "satanic staircase" seen more clearly (complete). In this phase 2/7 structure is dependent on the prehistory combination phases  $\approx 1/3$  and  $\approx 1/4$ . N-phase is a mixture of long-period phase with a small admixture of chaotic. As the pressure increases in J<sub>c</sub> and M phases, the number of energetically equivalent sets of long-period and chaotic phases, according to [13], may increase. The phase transition in this case represent the areas where change is carried out medium wave vector. We can assume that the phase transition M<sub>1</sub>  $\ll$  M<sub>2</sub> is a change of the wave vector q<sub>s</sub> chaotic structure of 1/4 to 1/5 or 1/6 through the intermediate value type q<sub>s</sub>  $\approx 0.222 \approx 1/4$ -d. Therefore, diffraction techniques can be observed here another narrow phase, as predicted by the model Aubrey [12] and have been reported in (NH<sub>4</sub>)<sub>2</sub>ZnCl<sub>4</sub> [47,50] and (NH<sub>4</sub>)<sub>2</sub>ZnBr<sub>4</sub> (Figure 1.6).

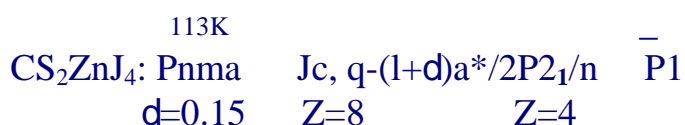
Shape of the resonance lines in the incommensurate phase may reflect a certain type of mixed between states q<sub>d</sub>  $\approx 1/4$  and q<sub>d</sub>  $\approx 1/3$  of the nonlinear solutions.

Thus, the comparison of the theoretical phase diagrams with P-T diagram of the NQR data and taking into account the data neutron diffraction scattering, suggesting that an increase in pressure in the RZB should be observed structure type 1/5, 1/6, 1/8 and etc., approaching the Lifshitz point. As for structural changes in phase modulated, one can assume the presence of a substantial Rb<sub>2</sub>ZnBr<sub>4</sub> interactions frustrating crystal spatial symmetry. Framework for describing transformation of the structure and evolution of the NQR spectra, from this point of view, should be sought in the implementation of competition electrical interaction between the sublattices of the structure and its

connection with the phonon spectrum. Availability the nonlinear polarization in this class of compounds has long been established. It is due to significant distortion and rotation groups  $BX_4$  and inhomogeneous polarization of the electrons in the atomic core. In this connection there are substantial electric dipole moments of atomic groups, the values of which differ for each group in both magnitude and direction. Accounting for such a spatially inhomogeneous nonlinear electrical deposits can significantly change the way in the shape description resonance spectra in the compounds of the family  $A_2BX_4$ . Cause of heterogeneity to be found in the intricacies of the nature of the chemical bond.

Finally, we can also make a comparison of theoretical phase diagram Aubrey with experimental data on change in the magnitude of the wave vector  $q_d$  in other compounds  $A_2BX_4$  (Table 4.1).

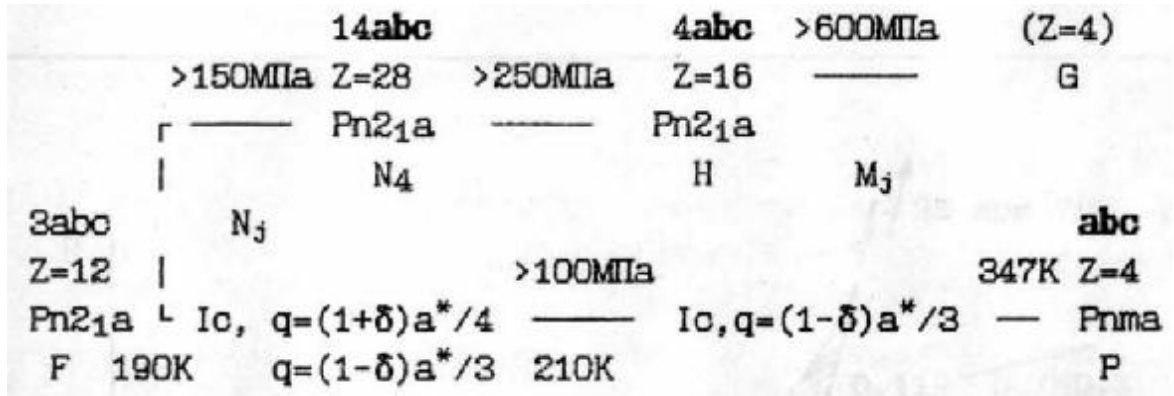
From the point of view of crystal chemistry, the relative magnitude of the radius of the cation A compound  $A_2BX_4$  can be divided into two groups. In the first group, with a large cation Cs, the following sequence transforming structures:



In  $Cs_2CdJ_4$ ,  $Cs_2CdBr_4$  sequence transformation structures and size  $q_d$  in Jc close to those for  $Cs_2CdJ_4$ . In the second group, with medium and small radius of the cation, there is a different sequence of transformations of the structure, characterized by low-temperature phase with the space group  $Pn2_1 a$ , but with different multiplicity of the unit cell volume relatively high. So for  $Rb_2ZnBr_4$  under pressure, we have:

**Table 4.1. Modulation Character and evolution of the family structure in crystals  $A_2BX_4$  -type structure b- $K_2SO_4$ .**

$K_2SeO_4$ (Pnma) Z=4	129K	$Jc, q = (1-\delta)a^*/3$ $\Sigma$ линия	$\longleftrightarrow$	93K	$Pn2_1a$
$K_2ZnCl_4$ (Pnma)	553K	$Jc(0,3233 < q < 0,330a^*)$	$\longleftrightarrow$	403K	$Pn2_1a$ Z=12
				145K	ИЛИ $P11a$ $Aa11$ Z=24, $1/2(b^*+c^*)$
$Rb_2ZnCl_4$ (Pnma) Z=4	302K	$Jc(0,3233 < q < 0,3283)$	$\longleftrightarrow$	189K	$Pn2_1a$ Z=12
				74K	$P1a1$ ИЛИ $Aa11$ Z=24
$Rb_2ZnBr_4$ (Pnma)	347K	$Jc(0,295 < q < 0,3310)$	$\longleftrightarrow$	200K	$Pn2_1a$ Z=12
Z=4 a, b, c		$\approx 3a, b, c; \Sigma$		108K	$Pn2_1a$ утроение 3a, b, c
				80K	$P1c1$ Z=12 50K ↓ 3abc
$Cs_2CdBr_4$ Pnma	252K	$Jc[q \approx 0,15a^*]$ Г-точка Л-линия	$\longleftrightarrow$	237K	$P2_1/n$ Z=4
				156K	$P\bar{1}$
$Cs_2HgBr_4$	243K	$Jc[q \approx 0,15a^*]$ Г-точка	$\longleftrightarrow$	230K	$P2_1/n$ Z=4
				165K	$P\bar{1}$ Z=4
				84K	$P\bar{1}$ Z=8
$(NH_4)_2ZnCl_4$ Pnma	402K	$Jc(q=2/7a^*)$ $\Sigma$	$\longleftrightarrow$	276K	$P112_1$ $Pn2_12$ Z=16
	365K			271K	
				266K	$Pn2_1a$ Z=12
				80K	↓ 55K триклин.
$(NH_4)_2ZnBr_4$ Pnma Z=4	428K	$Jc(q=2/7a^*)?$	$\longleftrightarrow$	222K	$Pn2_1a$ Z=16
				218K	$Pn2_12$ Z=12
$(TMA)_2ZnCl_4$ Pnma Z=4	296K	$Jc(q=(2/5+\delta)a^*)$ $q \approx 0,42a^*$	$\longleftrightarrow$	200K	$Pn2_1a(q=2/5a^*)$ Z=20
				275K	$P2_1/n$ Z=12
				168K	↓ $P12_1/c1$ Z=4 ↓ 155K $P2_12_12_1$ (Z=12)
$(NH_4)_2BeF_4$ Pnma Z=4	183K	$Jc(q=(1-\delta)a^*/2)$ Z=12	$\longleftrightarrow$	177K	$Pna2_1(C_{2v}^9)$ удвоение по a
$NaNO_2$	107K	$Jc(q \text{ от } 1/5 \text{ до } 1/8 \dots)$	$\longleftrightarrow$	108K	$C_{2v}^{20}$
$SC(NH_2)_2$		$Jc(q \text{ от } 1/7 \text{ до } 0)$	$\longleftrightarrow$	108K	утроение
	↓218K	$q \text{ от } 0,141 \text{ до } 0,115$	$\longleftrightarrow$	193K	$q=1/9$
				191K	$P2_1ma$



From a comparison of the amount of change of the wave vector  $q_d$  within the incommensurate phase at atmospheric pressure (Table 4.1) compounds  $A_2BX_4$  and taking into account the data for  $\text{Cs}_2\text{CdJ}_4$ ,  $\text{Cs}_2\text{ZnJ}_4$  and  $\text{Rb}_2\text{ZnBr}_4$  under pressure, we can put isobaric line atmospheric temperature change of each compound from Table. 4.1 the theoretical phase diagram and Aubrey Buck. As a result, we obtain the circuit (Fig.4.40), where through the line marked by the particular compound  $A_2BX_4$  are isobaric atmospheric line  $q_d$  experimental measurements in this compound, and the oval area outlined by dashed lines represent stylized model Aubrey polyhedra [12], where the period of the structure does not change, but changes the phase shift between the sublattices model.

As can be seen from the presented scheme, despite unconfirmed some experimental data or their limitations, there is sufficient correlation between the known experimental P-T phase diagrams of the generalized phase diagram of Scheme Fig.4.40. Please keep in mind that the cesium compound was isolated as a subclass, characterized by a specific sequence of symmetry transformations associated with the softening of the phonon spectrum near the **T** point of the Brillouin zone, and the rest - in the subclass - along **S** line.

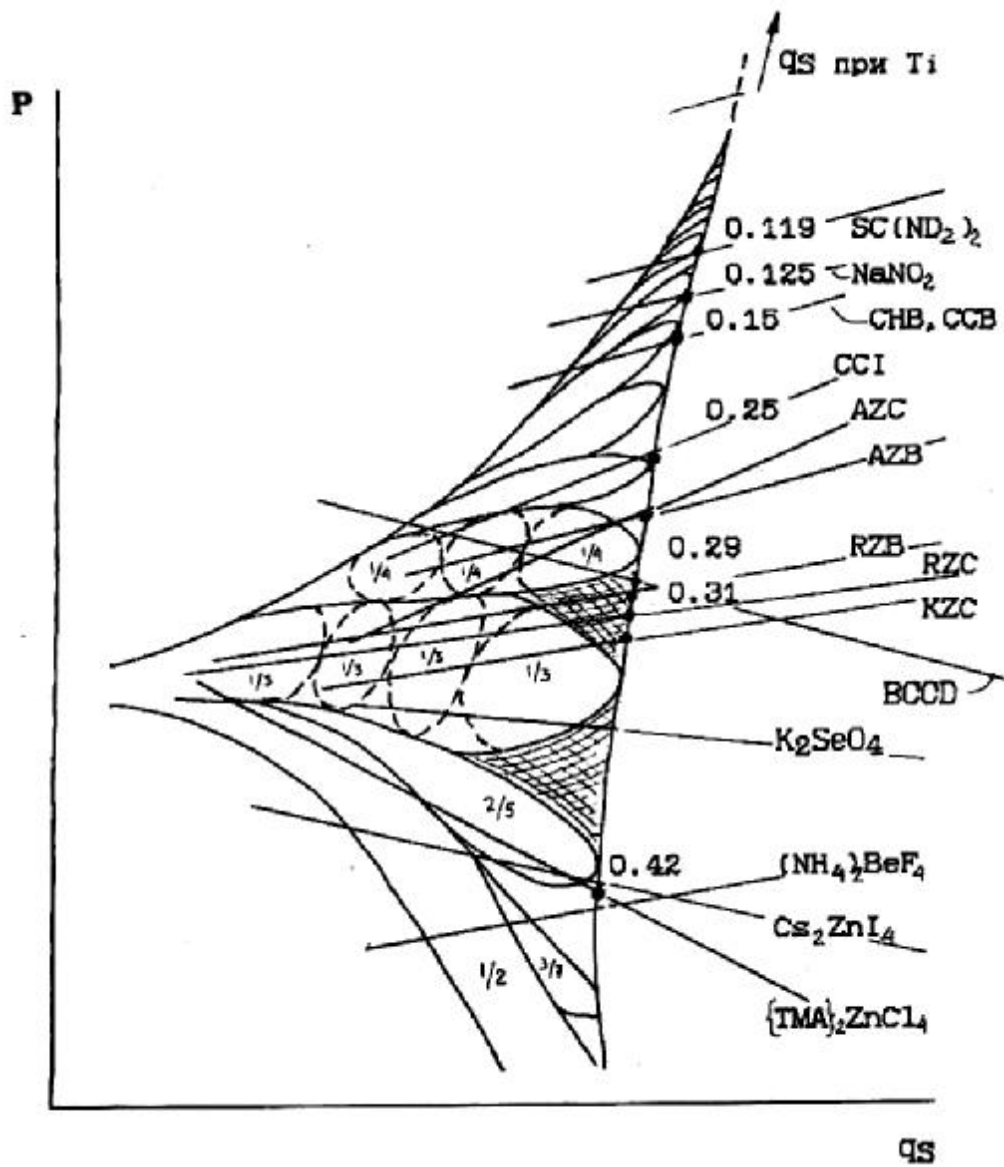


Fig.4.40. Comparison of experimental data on the change of the wave vector  $q_d$  in various compounds such  $\beta$ -K<sub>2</sub>SO<sub>4</sub> with the theoretical phase diagram [12].